Chapter 4

Reduced Order Modelling

In the previous chapter the state space representation of the microgrid system was considered under the consideration such that the AC microgrid is in autonomous and grid-tied mode. The derived models are of 36^{th} and 15^{th} order system respectively. Besides this the DC microgrid state space model with PV-fuel cell is a 38^{th} order complex system. With multiple DERs being interconnected the complexity increases exponentially, which makes the design and analysis indispensable. Model Order Reduction is basically a methodology which tries to reduce the order of a complex system to appreciably cut down the computational time and substantially reduce the cost and storage requirements. An accurate reduced order model is capable of interpreting a complex system efficiently in the time and frequency domains, without compromising the salient features of the system. A theoretical procedure for the reduced order modelling of the previously obtained microgrid models has been discussed in this chapter which can be applied for similar microgrid configurations. This chapter also deals with the lower order equivalents with the original small signal models in comparison of the simulation of the two systems. These results have been verified in Typhoon HIL 402 real time emulator.

4.1 Preliminaries

Few of the concepts of reduced order modelling significant to the analysis in this chapter have been discussed prior to their implementation for order reduction to the complex microgrid systems.

4.1.1 Norm based error reduction

The general MOR problem statement consists of a higher order LTI system $G(s)$ of order n to be reduced to a lower order system $\hat{G}(s)$ of order r (r<n), such that $||G(s) - \hat{G}(s)||$ is small; where $||.||$ is norm based distance measure. These system norms used in MOR problems are generally of three standard forms; L_1 norm, H_2 norm and H_∞ norm.

Considering the error signal as $e(t)$, the system norms can be defined in the context of MOR as follows [63].

For $e(t) = g(t) - g_r(t)$ in time domain and $E(s) = G(s) - \hat{G}(s)$ in laplace domain,

where $L^{-1}\left(\hat{G}(s)\right) = g_r(t)$ and $L^{-1}\big(G(s)\big) = g(t)$,

L_1 norm is the integral of the absolute error time responses defined as;

$$||error||_{1,f} = \int_0^\infty |g(t) - g_r(t)|dt \tag{4.1}$$

where, f is a step, impulse or ramp function.

H_2 norm gives the RMS value of system response to white noise and represents the tracking error. It is defined as;

$$||error||_2 = \int_0^\infty e^T(t)e(t)dt \tag{4.2}$$

H_∞ norm is the maximum gain of the error function in frequency domain. It is expressed as; $\|error\|_\infty \triangleq max\ \bar{\sigma}\big(E(j\omega)\big)\ \forall\omega$ (4.3)

The weighted sum of these error norms is termed as *Mixed Norm*. The mixed norm utilizes the combined advantages of more than one system norms to achieve multiple

objectives such as error rejection, robustness, performance, noise attenuation etc. in reduced order modelling [61]. It can be expressed mathematically as;

$$J = m * H_2\ norm(E) + n * H_\infty\ norm(E) + p * L_2\ norm(E) \tag{4.4}$$

where, m, n and p are the proportionality weights of the norms.

4.1.2 Dominant pole retention

Few of the main methods in MOR that are utilised for reduced order modelling of microgrid system have been discussed here. Order of a transfer function can be reduced by retaining its dominant poles in the reduced transfer function. Poles which are nearest to the origin are retained depending on the order to be reduced. Thus an implication can be drawn about the overall behaviour of the reduced system which will be pretty much similar to the original system. This is so because the contribution of the un-retained eigenvalues to the system response are essential only at the initiation of the response, whereas the eigenvalues retained are essential throughout the whole response. It is in fact, these eigenvalues that determine the type of the response of the system [36]. Mathematically, dominance is defined in [82] in terms of weighted residue defined as;

$$\rho_i = \frac{|R_i|}{|Real(\lambda_i)|} \tag{4.5}$$

where, R_i denotes the residue of the eigenvalue λ_i. Thus an eigenvalue λ_i is dominant if $\rho_i > \rho_j$, for all $i \neq j$.

4.1.3 Direct and Balanced Truncation

Direct truncation is a straightforward method of MOR which directly truncates the transfer function to desired order for a multivariable system. For the n^{th} order transfer function in (4.6), its direct truncation equivalent to 2^{nd} order is given in (4.7).

$$G_{ij}(s) = \frac{b_{n-1}s^{n-1}+b_{n-2}s^{n-2}+\cdots.+b_0}{a_n s^n+a_{n-1}s^{n-1}+\cdots.+a_0} \tag{4.6}$$

$$G_{ij,2}(s) = \frac{b_1 s+b_0}{a_2 s^2+a_1 s+a_0} \tag{4.7}$$

Balanced Truncation method is the solution that is provided by the Lyapunov equations as the controllability and observability Gramian matrices W_C and W_O [35] which are symmetric positive semi-definite; such that,

$$\boldsymbol{AW_C + W_C A^T = -BB^T} \tag{4.8}$$

$$\boldsymbol{A^T W_O + W_O A = -C^T C} \tag{4.9}$$

Balanced system implies that the Gramians are equal and diagonal, i.e., for a stable and minimal system, the condition of balance is as in (4.10).

$$\boldsymbol{W_C = W_O} = diag(\sigma_1, \sigma_2, \ldots\ldots, \sigma_n) \tag{4.10}$$

In case of unbalanced system realisations, the similarity transformation of these matrices is used for the system analysis. As far as the MOR is concerned, the condition for balance in a system is approached by the removal of those states of the system that are hard to control i.e. they need a large amount of energy in order to control them. Moreover the problem that they are difficult to observe as they yield a small amount of energy. Hankel Singular Values (HSVs) of the system [85] as discussed in the next subsection, helps determine these states which are to be eliminated for order reduction in the subsequent analysis.

Inspite of the superiority of Balanced Truncation in the applications of power systems which is owed to its mathematical basis over wide ranges of frequencies, the major drawback to this approach is the occurrence of an instability when it comes to larger systems and also large values of steady state errors [35].

4.1.4 Hankel Singular Value (HSV)

The mathematical formula of HSV is derived as the square root of the eigenvalues of the Gramian product matrix (positive), as

$$\boldsymbol{\sigma_m} = \sqrt{eig(\boldsymbol{W_C W_O})} \tag{4.11}$$

where, $m=1,2,\ldots,n$(no. of system states).

In reduced order modelling, the HSV of the larger system determines the underlying energy level of the states so that the states with higher energies are retained whereas those with low energy are completely removed without hindering the overall system balance. The HSV plot gives a graphical view of the dominant states and aids in determining the degree of reduction. This HSV plot has been used in further analysis and can be observed in the Section 3.3 of 'Simulation results'.

4.1.5 Evolutionary Algorithms (EAs)

The basic concept and dominant characteristics of EAs as in [50] is depicted as a vying between a population of individuals which causes natural selection (survival of the fittest) under the influence of environment which is leading to the rise in fitness of population. The main features of EAs are;

- EAs are based on population, i.e., they operate on an entire set of candidate solutions simultaneously.
- EAs generally apply the technique of recombination to achieve combined information from various candidate solutions to develop a new and better solution.
- EAs are stochastic tools of optimization.

Evolutionary Algorithms are increasingly being used in optimal MOR of complex systems due to their inherent adaptive and robust nature. In this work, these EAs are used for error function (4.27) minimization. Basically the agent-based Swarm Intelligence (SI) techniques [47] have been employed for minimization of error norm in reduction process. The robustness and added credibility in the SI techniques which can be accredited to the multi-agent, self-organisation, distributed and adaptive control features significantly increases their scope and potential for application in practical optimization problems and hence are discussed briefly in this section.

4.1.5.1 Particle Swarm Optimization (PSO)

PSO, a forerunner of the Artificial Bee Colony (ABC), which was developed by Eberhart and Kennedy, has been used for almost thirty years as one of the most popular optimization tool in various scientific problems [48]. In the PSO algorithm, a collection of particles which is termed as 'swarm', placed randomly in search space of the optimization problem. These particles move in a manner which is identical to movement of flock of flying birds in nature in search of food and shelter. Then for some predefined number of repetitions, the objective or fitness function of each particle is evaluated with their movements towards positions with better fitness. These movements are based on the particles own history of best location in context of fitness and with respect to the best positions attained by other particles in the group, and some inertia from current position with some random perturbations. Thus, the swarm obtains the most optimum pattern or solution to the fitness function in the problem space with a specified number of particles working in synchronisation [86]. This is the collaborative and mutually interactive swarm behaviour helps to attain the desired optimum within the restrictions of stipulated time

and resources. This tool results in higher flexibility and higher accuracy, which in turn helps to achieve the desired optimality with simple iterative programming.

Basically, PSO algorithm constitutes a swarm of particles, i.e., *n* particles and candidate solutions are presented by the position of each of the particle in the swarm with optimal fitness function in the *D*-dimensional search space. The particle alters its position in accordance to three factors [49], namely: its own inertia, its personal best optimal position and the swarm's best optimal position.

Figure 4.1. shows the flowchart of PSO algorithm [87].

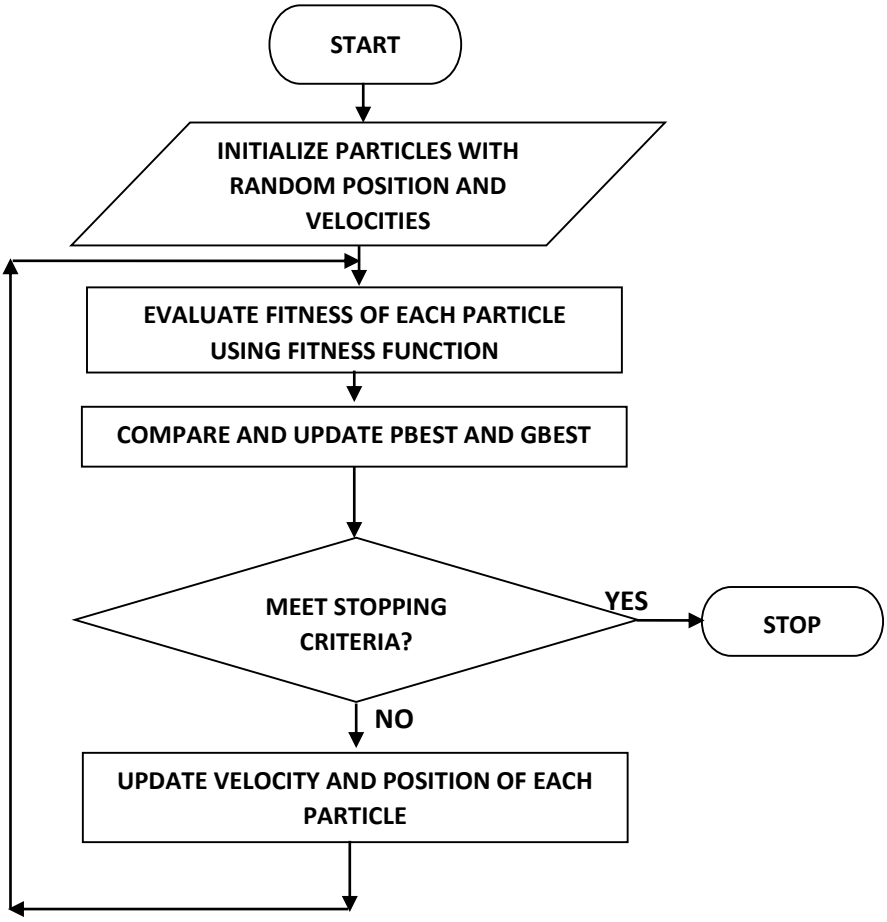

Figure 4.1. *Flowchart of PSO*

The PSO update rule equations are given as;

$$v_{id}^{k+1} = wv_{id}^{k} + c_1 r_1^k (pbest_{id}^{k} - x_{id}^{k}) + c_2 r_2^k (gbest_{id}^{k} - x_{id}^{k}) \tag{4.12}$$

$$x_{id}^{k+1} = x_{id}^{k} + v_{id}^{k+1} \tag{4.13}$$

where,

v_{id}^{k} and x_{id}^{k} representing the velocity and position of the i^{th} particle (out of n particles) at d-dimension (out of D dimensions) in the k^{th} iteration respectively.

$pbest_{id}^{k}$ and $gbest_{id}^{k}$ represent the personal best position that is achieved and global best position (i.e. group's best) of i^{th} particle (out of n particles) at d-dimension (out of D dimensions) in k^{th} iteration respectively.

w represents inertial weight attached to the particle's previously attained position;

c_1, c_2 represent acceleration constants;

r_1^k, r_2^k represent random numbers in the range of [0,1].

Thus, velocity update rule of PSO as in (4.12-4.13) largely contains three parts [88]:

Momentum: It represents the propensity of particle to keep the same movement alive as it was moving in the previous algorithm run. It represents the impact of particle's previous velocity on its current velocity.

Cognitive part: It resembles the movement of the particle towards its own personal best (pbest) position achieved so far. Referred to as "memory", "self-knowledge" or "remembrance".

Social part: It represents the movement of the particle towards swarm's best (gbest) position in terms of optimal fitness value. Referred to as "cooperation", "social knowledge" or "shared information".

The flexibility, simple computations and high convergence rate in PSO based reduction technique yields a well-organised and cost-effective lower order model which gives a good proximityof the result to its full-order original system.

4.1.5.2 Artificial Bee Colony (ABC)

In 2005 Dervis Karaboga had developed Artificial Bee Colony algorithm which was a multivariable and multimodal problem-solving algorithm. It had behaviour which was similar to other techniques of swarm intelligence [55]. This popular and widely accepted algorithm is based on the behavioural pattern of three type of bees in the bee colony which largely differ in their functionality: Depending on the roles they perform they are named as Scout bees, Employed bees and Onlooker bees [56-58]. In their natural environment, the employed bees explore a wide area in search of food and the onlooker bees carry out an analysis on the quality and credibility of the information about the nectar that is brought by employed ones to the bee colony. This is communicated in the form of the waggle dance. When the information brought by employed bees becomes indifferent in several runs then only the scout bees become active. Assuming those specific food sources to be abandoned, scouts then choose a random food source and the process goes on.

The basis of the ABC algorithm starts by the assumption of a population of particles or bees, *'2N'*, situated in search space such a manner that the number of employed bees and onlookers bees are equal. Scout bee can be portrayed as an employed bee of an abandoned resource. The flowchart in Figure 4.2. consists of three stages: stage one- Employed bee stage, second stage- Onlooker bee stage and the third stage- Scout bee stage. These three phases of ABC work in repetition and in perfect tandem for a predefined number of iterations which is denoted as, $Maxiter$, this is also the criteria for

the algorithm to stop. It is evident that these three parameters which are crucial for the algorithm are: $Maxiter$, limit and number of food sources, N. The equations used in the algorithm are given in (4.14-4.16).

$$v_{ij} = x_{ij} + \emptyset_{ij}\left(x_{ij} - x_{kj}\right) \forall\, k \neq i \tag{4.14}$$

where, $i \in \{1,2,..,N\}$, N is the number of food sources and $j \in \{1,2,..,d\}$, d is the dimension of particle location or number of unknown variables to be optimized, $\emptyset_{ij} \in [-1,1]$.

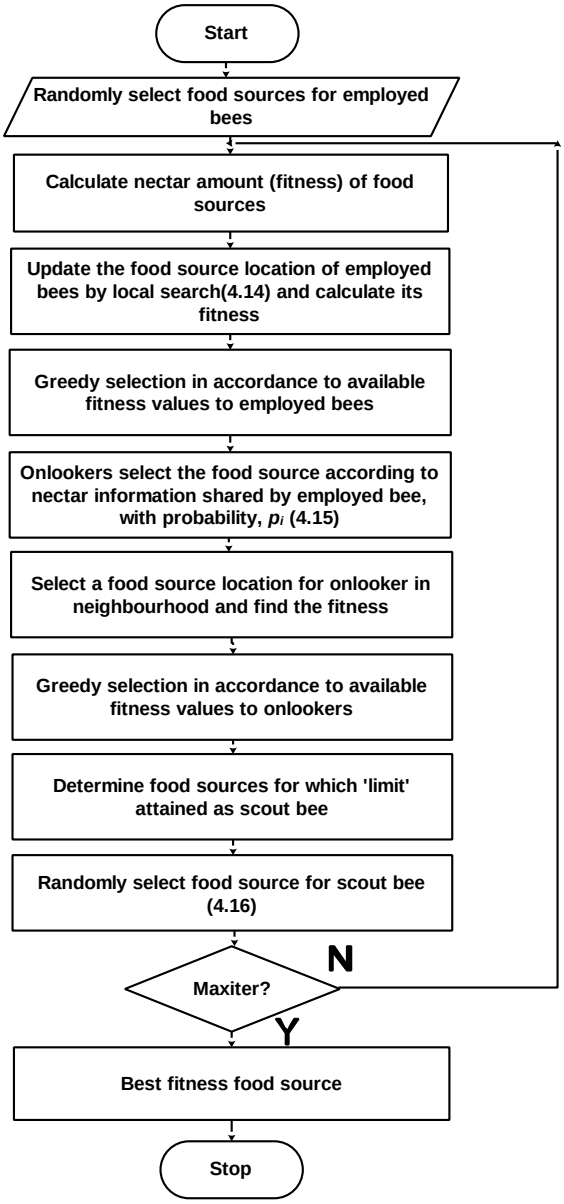

Figure 4.2. *Flowchart of the ABC algorithm.*

$$p_i = \frac{fitness_i}{\sum_{i=1}^{N} fitness_i} \tag{4.15}$$

where, $fitness_i$ is the fitness of i^{th} solution.

$$x_{ij} = x_{min,j} + \varphi_j\left(x_{max,j} - x_{min,j}\right) \tag{4.16}$$

where, $x_{ij} \in [x_{min,j}, x_{max,j}]$ and φ_j is a random number from 0 to 1.

4.1.6 Concept of Time-Scale Separation

Singular Perturbation theory encompasses the dynamical systems in which the scales of state dynamics are diversified. A small positive parameter is multiplied to some of the states to demonstrate the existence of different time scales in same system [89]. Consider a small parameter, ϵ, multiplied by state derivatives, such that;

$$\dot{x} = f(x, z, u, t, \epsilon) \qquad x(t_0) = \xi(\epsilon) \tag{4.17}$$

$$\epsilon\dot{z} = g(x, z, u, t, \epsilon) \qquad z(t_0) = \zeta(\epsilon) \tag{4.18}$$

Singular Perturbation analysis of the above system is actually the study of the behaviour of the system solution as $\epsilon \to 0$ and $0 < t < +\infty$. This small parameter divides the system into fast and slow subsystems such that, the slower subsystem dynamics are retained into the overall system dynamics for longer system operating times. Reduced order modelling through time-scale separation is based on the concept of elimination of fast states or their representation by an equivalent reduced order form such that the key information from fast subsystem is retained in the overall reduced order system. This concept has been deployed in the reduced order modelling of DC microgrid model in this thesis work, such that the slow subsystem is retained whereas the fast subsystem is reduced to retain the significant information which is added back in the overall reduced order model.

4.2 Optimal Model Order Reduction of Microgrid System

The order of the complex microgrid model is reduced to obtain a lower order equivalent with behaviour similar to the original system. This section has been divided into two parts of "Reduced Order Modelling of AC Microgrid" and "Reduced Order Modelling of DC Microgrid" so as to demonstrate different approaches for the order reduction of the two microgrid structures.

4.2.1 Reduced Order Modelling of AC Microgrid

Reduced order modelling of the higher order AC microgrid model in Chapter 3 to their lower order counterpart can be achieved by a number of classical and modern methods some of which are given in Section 4.1. The small signal model of AC microgrid in autonomous and grid-tied mode as in (3.43-3.44, 3.67), represents 36^{th} and 15^{th} order complex systems which are to be simplified while preserving the vital system characteristics. Mixed method consisting of pole retention and error minimization through artificial intelligence have been used for MOR of AC microgrid system in both autonomous and grid-tied mode. The problem formulation for this analysis is discussed in this section.

4.2.1.1 Transfer function modelling of AC microgrid in autonomous mode

The present work utilizes the transfer function model for reduced order modelling so as to visualise the dominant poles in s-plane and develop reduced order response for any input signal. The overall transfer function model of autonomous microgrid (3.43-3.44) with outputs i_{oDQ1}, i_{oDQ2}, ω_{PLL1}, $\omega_{PLL2}$and inputs $v_{bD1}, v_{bQ1}, v_{bD2}, v_{bQ2}$, is represented by 24 transfer functions from all inputs to outputs, given below;

$$\boldsymbol{G(s) = C(sI - A)^{-1}B} = \begin{bmatrix} G_{11}(s) & G_{12}(s) & G_{13}(s) & G_{14}(s) \\ G_{21}(s) & G_{22}(s) & G_{23}(s) & G_{24}(s) \\ G_{31}(s) & G_{32}(s) & G_{33}(s) & G_{34}(s) \\ G_{41}(s) & G_{42}(s) & G_{43}(s) & G_{44}(s) \\ G_{51}(s) & G_{52}(s) & G_{53}(s) & G_{54}(s) \\ G_{61}(s) & G_{62}(s) & G_{63}(s) & G_{64}(s) \end{bmatrix} \tag{4.19}$$

where, $G_{ij}(s)$ is the transfer function between i^{th} output and j^{th} input, given as;

$$G_{ij}(s) = \frac{N_{ij}(s)}{DC(s)} \tag{4.20}$$

$DC(s)$is the 36th order common denominator,

$N_{ij}(s)$is the numerator of the transfer function $G_{ij}(s)$.

Table 5.1. in Chapter 5 tabulates all the 36 common poles of $DC(s)$ with their damping ratios and oscillatory frequencies obtained from their real and complex parts. Considering the reduced order transfer function model of (4.19) as,

$$\boldsymbol{G_r(s) = C_r(sI - A_r)^{-1}B_r} = \begin{bmatrix} G_{r11}(s) & G_{r12}(s) & G_{r13}(s) & G_{r14}(s) \\ G_{r21}(s) & G_{r22}(s) & G_{r23}(s) & G_{r24}(s) \\ G_{r31}(s) & G_{r32}(s) & G_{r33}(s) & G_{r34}(s) \\ G_{r41}(s) & G_{r42}(s) & G_{r43}(s) & G_{r44}(s) \\ G_{r51}(s) & G_{r52}(s) & G_{r53}(s) & G_{r54}(s) \\ G_{r61}(s) & G_{r62}(s) & G_{r63}(s) & G_{r64}(s) \end{bmatrix} \tag{4.21}$$

where, $G_{rij}(s)$ is the transfer function between output i^{th} output and j^{th} input with order 'r' where (r<36);

$$G_{rij}(s) = \frac{N_{rij}(s)}{DC_r(s)} = \frac{b_{r-1}s^{r-1} + b_{r-2}s^{r-2} + \cdots . + b_0}{a_r s^r + a_{r-1}s^{r-1} + \cdots . + a_0} \tag{4.22}$$

$DC_r(s)$is the rth order common denominator,

$N_{rij}(s)$is the numerator of the transfer function $G_{rij}(s)$.

4.2.1.2 Transfer function modelling of AC microgrid in grid-tied mode

In a similar procedure, the state space representation of grid-tied microgrid model with nine outputs as $\Delta P, \Delta Q,\ \Delta i_{od}, \Delta i_{oq}, \Delta i_{ld}, \Delta i_{lq}, \Delta v_{od}, \Delta v_{oq}, \Delta \omega_{PLL}$ and the required

active and reactive powers, P^r, Q^r; as input can be given as a set of eighteen 15th order transfer functions (4.23) to relate each input to output in transfer function model. These derived transfer functions are employed in the reduced order modelling in subsequent analysis.

$$\boldsymbol{G(s) = C(sI - A)^{-1}B} = \begin{bmatrix} G_{11}(s) & G_{12}(s) \\ G_{21}(s) & G_{22}(s) \\ G_{31}(s) & G_{32}(s) \\ G_{41}(s) & G_{42}(s) \\ G_{51}(s) & G_{52}(s) \\ G_{61}(s) & G_{62}(s) \\ G_{71}(s) & G_{72}(s) \\ G_{81}(s) & G_{82}(s) \\ G_{91}(s) & G_{92}(s) \end{bmatrix} = \frac{1}{DC(s)} \begin{bmatrix} N_{11}(s) & N_{12}(s) \\ N_{21}(s) & N_{22}(s) \\ N_{31}(s) & N_{32}(s) \\ N_{41}(s) & N_{42}(s) \\ N_{51}(s) & N_{52}(s) \\ N_{61}(s) & N_{62}(s) \\ N_{71}(s) & N_{72}(s) \\ N_{81}(s) & N_{82}(s) \\ N_{91}(s) & N_{92}(s) \end{bmatrix} \quad (4.23)$$

where, $G_{ij}(s)$ is the transfer function between i^{th} output and j^{th} input given as;

$$G_{ij}(s) = \frac{N_{ij}(s)}{DC(s)} = \frac{b_{n-1}s^{n-1} + b_{n-2}s^{n-2} + \cdots + b_0}{a_n s^n + a_{n-1}s^{n-1} + \cdots + a_0} \quad (4.24)$$

$DC(s)$ is the n^{th} order common denominator (here n=15),

$N_{ij}(s)$ is the numerator of the transfer function $G_{ij}(s)$.

The reduced order model of the microgrid system is considered as;

$$\boldsymbol{G_r(s) = C_r(sI - A_r)^{-1}B_r} = \begin{bmatrix} G_{r11}(s) & G_{r12}(s) \\ G_{r21}(s) & G_{r22}(s) \\ G_{r31}(s) & G_{r32}(s) \\ G_{r41}(s) & G_{r42}(s) \\ G_{r51}(s) & G_{r52}(s) \\ G_{r61}(s) & G_{r62}(s) \\ G_{r71}(s) & G_{r72}(s) \\ G_{r81}(s) & G_{r82}(s) \\ G_{r91}(s) & G_{r92}(s) \end{bmatrix} = \frac{1}{DC_r(s)} \begin{bmatrix} N_{r11}(s) & N_{r12}(s) \\ N_{r21}(s) & N_{r22}(s) \\ N_{r31}(s) & N_{r32}(s) \\ N_{r41}(s) & N_{r42}(s) \\ N_{r51}(s) & N_{r52}(s) \\ N_{r61}(s) & N_{r62}(s) \\ N_{r71}(s) & N_{r72}(s) \\ N_{r81}(s) & N_{r82}(s) \\ N_{r91}(s) & N_{r92}(s) \end{bmatrix} \quad (4.25)$$

where, $G_{rij}(s)$ is the transfer function between i^{th} output and j^{th} input with order 'r' (r<15);

$$G_{rij} = \frac{b_{r-1}s^{r-1} + b_{r-2}s^{r-2} + \cdots + b_0}{a_r s^r + a_{r-1}s^{r-1} + \cdots + a_0} \quad (4.26)$$

$DC_r(s)$ is the rth order common denominator.

4.2.1.3 Methodology for reduced order modelling

In this thesis research work the methodology followed for reduced order modelling of AC microgrid system involves two steps as given below.

Dominant Pole Retention

The principle of dominant pole method is to retain the eigenvalues closes to origin, hence retaining dominant time constants in the reduced model. Thus the first step is to identify the dominant modes in the small signal model which are to be retained in the reduced order model. That is, the common reduced order denominator polynomial, $DC_r(s)$ in (4.20, 4.24), is obtained by dominant pole method so as to retain the slower system dynamics contributed by poles nearer to the imaginary axis. The eigenvalues of the small signal model of AC microgrid in autonomous mode, highlighted in Table 4.1., are significantly closer to origin as compared to other ones, and thus, are preserved in the reduced order approximant. This table also lists all the eigenvalues with modal numbers. Thus, for a 9^{th} order reduced model, the modes taken from original system are; oscillatory modes: 10,11,12,13 and a non-oscillatory mode: 16. Similarly, the two dominant poles of AC microgrid model in grid-tied mode, highlighted in Table 4.1. can be seen to be at a depth of 10^{-6} as compared to the other thirteen eigenvalues of the system. The high residues of these poles make dominant pole retention technique highly suitable for the system under consideration.

Error minimization by artificial intelligence

The norm based reduction error in reduced order modelling can be minimized through optimization algorithms wherein, the numerator polynomial of the transfer function model, $N_{rij}(s)$ in (4.22), is determined such that the error norm between original and reduced order system is minimum. The error norm constitutes the objective function

that is to be minimized through iterative optimization algorithms. PSO and ABC algorithms are used for this purpose in this research work. The detailed objective function formulation aspects are given in the next section.

Table 4.1. Eigenvalues of AC microgrid model.

Autonomous Mode			**Grid-tied Mode**		
Eigenvalues	***Real part ± jImaginary part***		***Eigenvalues***	***Real part ± jImaginary part***	
3,4	-2500.55	12528.61	*1*	0	
5,6	-2499.78	12526.57	*2,3*	-3999.16	11138.14
7,8	-2321.49	11784.72	*4*	-8397.40	
9,10	-2317.90	11780.49	*5,6*	-765.64	11320.53
11	-7912.59		*7*	-462.03	
12	-7903.62		*8*	-391.43	
1,2	-375.00	376.60	*9*	-54.61	
13,14	-3333.33	376.60	*10*	-45.08	
15,16	-1666.67	376.60	*11*	-50.26	
19,20	-258.03	64.11	*12*	-50.26	
17.18	-257.55	60.96	*13*	-1.63	
21,22	-79.36	16.51	***14***	**-32.10×10^{-6}**	
23,24	-77.36	19.29	***15***	**-16.12×10^{-6}**	
25,26	**-10.61**	**7.84**			
27,28	**-0.47**	**6.04**			
29,30	**-1.28**	**4.62**			
31	**-2.12**				
32,33	**-50.24**	**0.03**			
34,35	-50.25	0.03			
36	0				

4.2.1.4 Objective function formulation

Optimal reduced order modelling presents an improved approach to MOR by incorporating the advantages of the optimization algorithms into order reduction problem. The improvisation is further achieved by application of optimization algorithms, in the lieu of formulation of appropriate objective function because of the high flexibility and accuracy.

In this case, the optimal model order reduction is basically a function optimisation problem. Both the algorithms discussed in Section 4.1, PSO and ABC offer versatility and easy implementation based on iterative programming. ABC algorithm achieves a remarkable trade-off between its exploration and exploitation capability by employing both scout bee and employed-onlooker bee respectively. However, PSO achieves this balance by a weighing mechanism such that, the inertia weight associated with particle's last speed is decreased linearly so as to explore wider areas in the beginning and nearby areas at later stages. The combined cognitive and social forces on every particle of the swarm, help in achieving the best optima with minimization of reduction errors.

Now for optimal model order reduction, the numerator $N_{rij}(s)$ as in (4.22, 4.26) is to be determined by optimization algorithms such that the error norm between original and reduced order system is minimum, i.e.,

$$J = |e| = \int_0^\infty |g(t) - g_r(t)| \tag{4.27}$$

where, $g(t) = L^{-1}(G(s))$, is the time response of original system;

$g_r(t) = L^{-1}(G_r(s))$, is the time response of reduced system.

Equation (4.27) represents the fitness function or objective function whose value is to be optimized by PSO or ABC optimization algorithms. This fitness or objective function has been considered as the L_1 norm of the error signal in case of AC microgrid MOR in this

research work. It can also be constituted as a mixed norm for achieving multiple design objectives (4.4) as shown in Figure 4.3. Thus, the minimization of this objective function ensures efficient reduced order modelling of complex higher order microgrid system which can be used for further analysis without loss of generality.

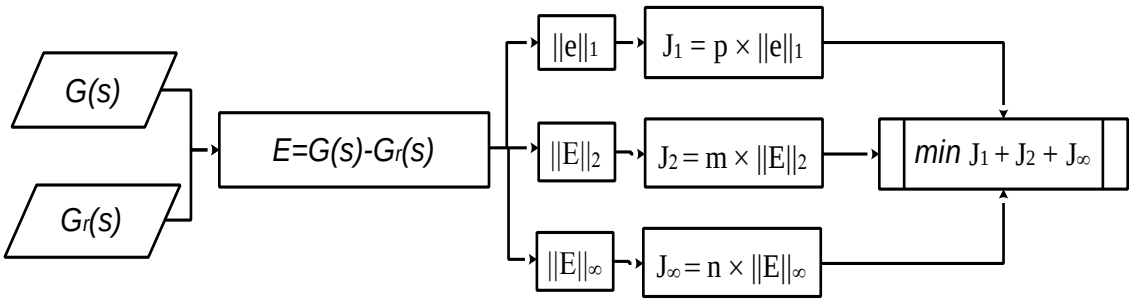

Figure 4.3. *Mixed norm based objective function formulation.*

The variables to be optimized by optimization algorithms are $b_{r-1}, b_{r-2}, \ldots b_0$ which are the coefficients of numerator polynomial $N_{rij}(s)$ in (4.22, 4.26), in the transfer function model of microgrid system both in autonomous and grid-tied modes, where r depends upon the degree of reduction. The extent of reduced order modelling of AC microgrid model, i.e., r has been determined by HSV plots and the results are given in Section 4.3.

4.2.2 Reduced Order Modelling of DC Microgrid

To demonstrate the concept of time-scale separation in reduced order modelling of complex power systems, the complexity of the autonomous PV-fuel cell based DC microgrid model derived in Section in Chapter 3 has been simplified in this research work by adopting timescale separation principle, where a wide range of timescales from millisecond to several seconds exists due to the slower chemical-electrochemical

processing in fuel cell. To completely retain the high nonlinearity in slower states that do exist in fuel cell system, it is kept intact, in the reduced order system model. The procedure followed for analysis is as in Figure 4.4.

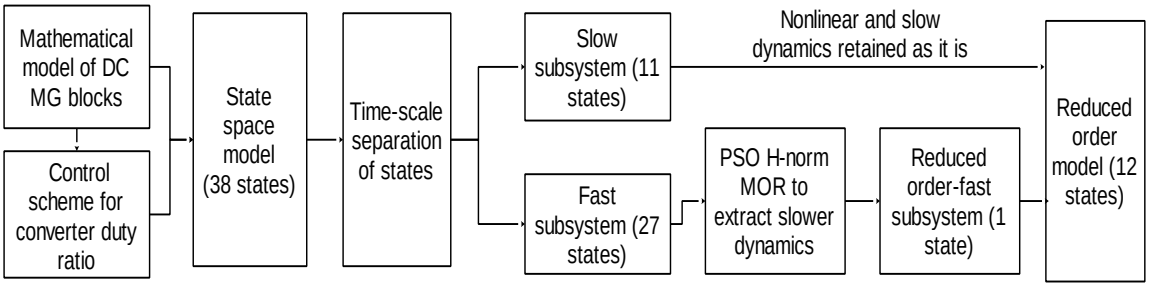

Figure 4.4. *Flow of process for reduced order modelling of DC microgrid.*

The reduced order modelling of fast subsystem extracts the most significant information which is added in the overall reduced order model in order to simplify the system without causing much change in its dynamics. This reduced fast subsystem representation can be obtained by any model order reduction techniques available in literature [8]. PSO being a versatile and elegant optimization technique and a strong candidate for optimization objective as discussed in Section 4.1, is adopted to obtain reduced system representation which almost replicates the full order system behaviour [49]. However, in order to address the impact of uncertainty due to stochastic and intermittent renewable resources in DC microgrid, a mixed H2 and H∞ norm discussed earlier in this chapter, has been formulated to solve the two-fold objective of reduced tracking error and increased robustness.

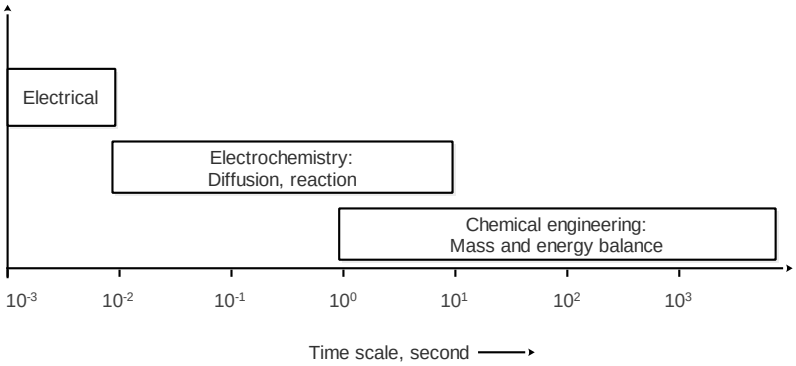

Figure 4.5. *Time scales in different dynamics*

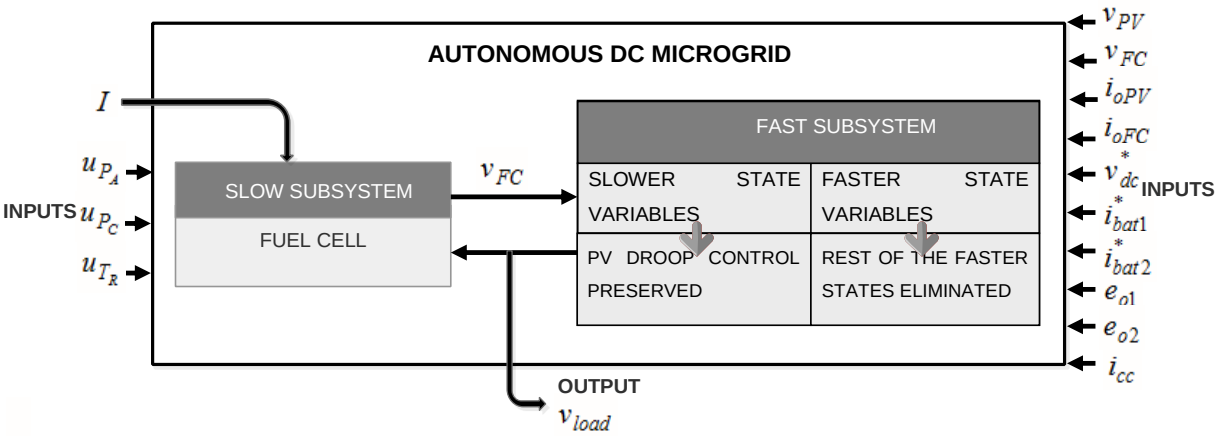

Figure 4.6. *Principle of time-scale separation used for DC microgrid system.*

4.2.2.1 Timescale separation of system states

The two-time scale separation in the state space of the considered architecture has been achieved on account of the distinct gap in the time responses of the fuel cell-chemical-electrochemical process states in comparison to the rest of the electrical system states as shown in Figure 4.5. The slower fuel cell dynamics presents an opportunity to accurately group the states associated with it into a slow subsystem. This also serves the purpose of retaining high nonlinearities in fuel cell dynamics. The rest of the states representing electrical quantities are grouped into a fast subsystem as shown in Figure 4.6. Thus, the state space of the overall system as in (26) in Chapter 3 is divided into two groups, x_{slow} and x_{fast}, given as;

Slow subsystem;

$$\boldsymbol{x_{slow}} = \boldsymbol{x_{fc}} = [(m_{O_2})_{net};\ (m_{H_2})_{net};\ (m_{H_2O})_{net};\ T;\ P_{H_2};\ P_{O_2};\ P_{H_2O};\ Q_C;\ Q_E;\ Q_L;\ v_{cd}] \quad (4.28)$$

Fast subsystem;

$$\boldsymbol{x_{fast}}$$

$$= [v_{oPV};\ v_{oFC};\ i_{L,PV};\ v_{c1,PV};\ v_{c2,PV};\ i_{L,FC};v_{c,FC};\ \emptyset_{pv};i_{opv,f};\ \mu_{pv};\ \eta_{pv};\ g_{v.pv};\ g_{c.pv};\ i_{ofc,f};\ \mu_{fc};\ \eta_{fc};$$

$$g_{v.fc};\ g_{c.fc};i_{bat1};\ i_{bat2};\ v_{c1,B};\ v_{c2,B};\ z_1;\ z_2;\ i_{line1};\ i_{line2};\ v_{load}] \quad (4.29)$$

The number of states in fast and slow subsystem is 27 and 11 respectively.

4.2.2.2 Objective function formulation for reduced order modelling of fast subsystem

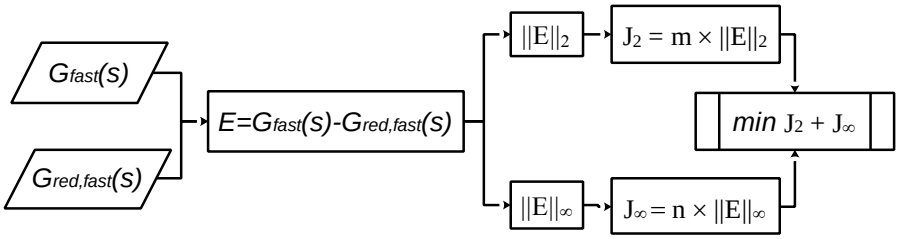

Figure 4.7. *Objective function formulation for fast subsystem of DC microgrid.*

The main objectives of reduced order modelling of the fast subsystem are to;

- Neglect the effect of faster dynamics associated with system state variables other that for fuel cell, that die out quickly in system response
- Extract the most significant information from the fast modes with highest participation factor.
- Sufficiently reduce the fast subsystem state space representation to reduce memory and time requirements.

The nonlinear state space representation of fast subsystem is linearized around stable operating points and obtained as in (4.30).

$$\dot{x_{fast}} = A_{fast}x_{fast} + B_{fast}u$$
$$y = v_{load} = C_{fast}x_{fast} \quad (4.30)$$

where, $C_{fast} = [0_{1\times 26}\ 1]$, u, x_{fast} are given in (4.29).

The reduced order modelling of state space model as in (25) into a simplified model, to be included in the reduced order model of DC microgrid system together with the slower subsystem, has been achieved by Evolutionary Algorithm based MOR techniques.

Mixed H-norm optimization by PSO algorithm utilises the two system norms: H_2norm and H_∞ norm to effectively obtain a simpler reduced representation of a large complex system in terms of order of the system. The renewable resources being used as important component of DC microgrid are stochastic and intermittent in nature, thus disturbance rejection as well as noise attenuation is indispensable in enhancing the efficacy of configuration being used. Moreover, as discussed in Section where H_2 norm represents RMS value of system response to white noise and H_∞norm is represents the largest frequency gain value of the overall system and hence, their combination provides a rich source of system information.

To represent the fitness function of PSO in terms of error function, the representation of 27-state subsystem is given as;

$$G_{fast}(s) = C_{fast}\left(sI - A_{fast}\right)^{-1} + B_{fast} \equiv \begin{bmatrix} A_{fast} & B_{fast} \\ C_{fast} & 0 \end{bmatrix} \quad (4.31)$$

The reduced order fast subsystem is similarly represented as;

$$G_{red,fast}(s) = C_{red,fast}\left(sI - A_{red,fast}\right)^{-1} + B_{red,fast} \equiv \begin{bmatrix} A_{red,fast} & B_{red,fast} \\ C_{red,fast} & 0 \end{bmatrix} \quad (4.32)$$

The error state-space E, between full order and reduced order state space representations is defined as;

$$E(s) = G_{fast}(s) - G_{red,fast}(s)$$

$$E = \left[\begin{array}{cc:c} A_{fast} & 0 & B_{fast} \\ 0 & A_{red,fast} & B_{red,fast} \\ \hdashline C_{fast} & -C_{red,fast} & 0 \end{array}\right] = \begin{bmatrix} A_E & B_E \\ C_E & 0 \end{bmatrix} \quad (4.33)$$

Let the optimizable parameters be denoted as, $A_{red,fast} = [a]$;

$B_{red,fast} = [b_1\ b_2\ b_3\ b_4\ b_5\ b_6\ b_7\ b_8\ b_9\ b_{10}];\ C_{red,fast} = [c]$

The Figure 4.7. shows the fitness function for PSO algorithm as weighted sum of two errors represented as mixed $H_2$and H_∞ error norms;

$$J = J_2 + J_\infty = m * H_2\ norm(E) + n * H_\infty\ norm(E) \quad (4.34)$$

where, $J_2 = \int_0^\infty e^T(t)e(t)dt$ represents the tracking error and $J_\infty = \|E(s)\|_\infty \triangleq max\ \bar{\sigma}\big(E(j\omega)\big)\ \forall\omega$ is a measure of the maximum gain of the transfer function.

Thus, minimization of objective function ensures reduced tracking error and increased robustness as any gain at the frequency of the highest value of a singular value plot can lead system unstable. Thus, the parameters to be optimized by optimization algorithm are: $a, b_1, b_2, b_3, b_4, b_5, b_6, b_7, b_8, b_9, b_{10}, c, m, n$.

4.3 Simulation Results

The reduced order model of microgrid systems have been simulated in MATLAB 2016a version and the optimization algorithms are simulated on Intel(R) Core™ i5-5200U CPU 2.20GHz (4.00 GB RAM). The optimal model order reduction of AC and DC microgrids are given in separate subsection below.

4.3.1 Optimal MOR in AC Microgrid

4.3.1.1 Reduced order modelling of AC microgrid in autonomous mode

The mathematical modelling with small signal analysis of the two inverter configuration as considered in this thesis is represented by 36 state variables. In practical systems, the autonomous microgrid consists of a large number of DERs interconnected to meet the load requirements of an area. Thus, the small signal model tends to become computationally more complex. The order of higher order transfer functions are dimensionally simplified by utilising the advantages of conventional dominant pole technique and PSO method. The common denominator polynomial is obtained by dominant modes as in Table 4.1. The overall reduced order model has been obtained such that the error norm in equation (4.27) is used as the fitness function of particles in multiple iterations of PSO algorithm. The various parameters used in PSO algorithm are given in Table 4.2.

Table 4.2. Parameters of the ABC Algorithm for AC microgrid in autonomous mode

Parameter	***Value***
No. of generations	150
Swarm size	40
c_1,c_2	2.2,2.1
[w_{max},w_{min}]	[0.9,0.4]

The time responses of the full order and reduced order transfer functions by balanced truncation and proposed technique are given in Figure 4.8. The reduced order step response of $\frac{\omega_{PLL1}(s)}{v_{bD2}(s)}$ shows a steady state error by balanced reduction. The ISE and ITAE to step inputs, in the resulting reduced order transfer function model is given in

Table 4.3. The transfer functions from v_{bD1} to ω_{PLL1} , ω_{PLL2} , as seen from the table, give better reduced order model by balanced truncation whereas, the other transfer functions give better results with the proposed method.

This table also gives the errors in reduction of the same system by balanced truncation approach. The step, impulse and ramp responses of PLL angular frequency in Figure 4.8.(a-c), show the dominance of the proposed method. Thus, the comparative analysis of these errors clearly indicates that the proposed method achieve better order reduction than the other method.

The changes in system dynamics due to perturbation (as in Figure 3.21.), in the initial time period of system responses, makes it necessary to analyse the reduce order modelling of the perturbed system as well. Though for small changes in eigenvalues due to this perturbation, the deviations in reduced order transfer functions for perturbed system will not be remarkable but still their magnified impact can be seen in Figure 4.9. This figure shows that the proposed reduction method is not only good for the earlier small signal model of microgrid, also gives a good approximation of perturbed microgrid systems as well.

The error norm in equation (4.27) of the reduced order model with different standard inputs: Unit impulse input $\delta(t)$, unit step input $u(t)$ and unit ramp input $r(t)$; for both system without uncertainty and system with uncertainty, for some of the transfer functions of the system are given in Table 4.4. The impulse error norm is seen to be higher than ramp and step error norm values.

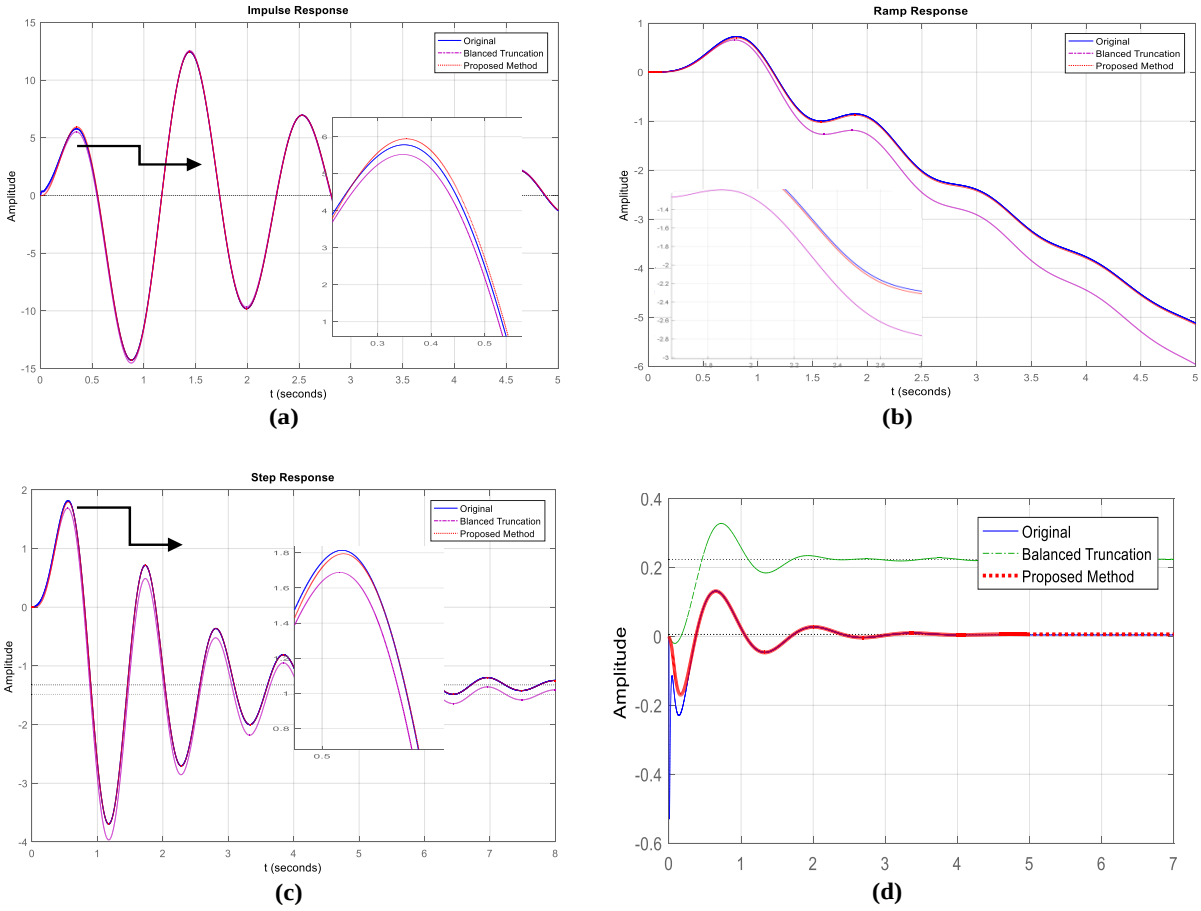

Figure 4.8. *Time responses of full order and reduced order autonomous microgrid system. (a) Impulse response (b) Ramp response (c) Step response of* $\frac{\omega_{PLL2}(s)}{v_{bQ1}(s)}$*, (d) Step response of* $\frac{\omega_{PLL1}(s)}{v_{bD2}(s)}$.

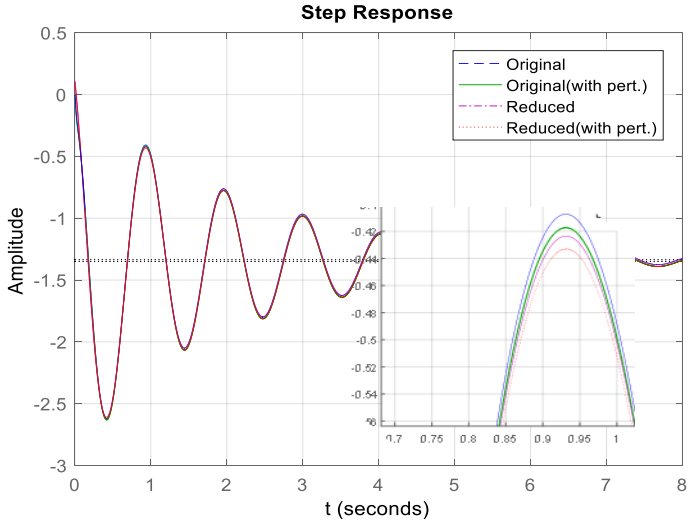

Figure 4.9. *Model order reduction of the perturbed and unperturbed transfer function* $\frac{i_{oQ1}(s)}{v_{bD1}(s)}$ *for AC microgrid in autonomous mode.*

Table 4.3. ISE and ITAE for all transfer functions for autonomous AC microgrid.

Transfer function	**ISE**		**ITAE**	
	BT	***Proposed***	***BT***	***Proposed***
$\boldsymbol{i_{OD1}(s)/v_{bD1}(s)}$	25.3748	22.4097	125.7981	106.4528
$\boldsymbol{i_{OQ1}(s)/v_{bD1}(s)}$	7.1662	5.6677	1148.3734	53.9848
$\boldsymbol{i_{OD2}(s)/v_{bD1}(s)}$	63.1841	3.0671	26.0544	22.9404
$\boldsymbol{i_{OQ2}(s)/v_{bD1}(s)}$	9.3897	5.2964	32.8778	47.8019
$\boldsymbol{\omega_{PLL1}(s)/v_{bD1}(s)}$	2.6144	5.8919	274.0537	194.6047
$\boldsymbol{\omega_{PLL2}(s)/v_{bD1}(s)}$	0.3021	1.1341	166.1873	127.2240
$\boldsymbol{i_{OD1}(s)/v_{bQ1}(s)}$	0.0782	0.0297	10.1155	7.2792
$\boldsymbol{i_{OQ1}(s)/v_{bQ1}(s)}$	2.0955	2.0779	42.2261	86.1811
$\boldsymbol{i_{OD2}(s)/v_{bQ1}(s)}$	0.7502	0.2190	53.0852	40.0971
$\boldsymbol{i_{OQ2}(s)/v_{bQ1}(s)}$	1.8197	1.1118	78.3357	32.6199
$\boldsymbol{\omega_{PLL1}(s)/v_{bQ1}(s)}$	11.7868	1.3624	1354.6428	175.0446
$\boldsymbol{\omega_{PLL2}(s)/v_{bQ1}(s)}$	2.8359	1.7320	807.2399	184.1313
$\boldsymbol{i_{OQ1}(s)/v_{bD2}(s)}$	1.9255	1.4104	3.0392	0.7847
$\boldsymbol{\omega_{PLL1}(s)/v_{bD2}(s)}$	4.9850	4.3867	17.9070	2.2281
$\boldsymbol{\omega_{PLL2}(s)/v_{bD2}(s)}$	26.9338	25.128	213.3036	63.8961
$\boldsymbol{i_{OQ1}(s)/v_{bQ2}(s)}$	0.07350	0.0522	9.5347	0.6392
$\boldsymbol{\omega_{PLL1}(s)/v_{bQ2}(s)}$	23.5205	1.4432	18.1278	1.4519
$\boldsymbol{\omega_{PLL2}(s)/v_{bQ2}(s)}$	15.3154	13.4021	27.3498	11.7831

Table 4.4. Impulse, step and ramp errors for AC microgrid transfer functions.

	Error Norm	$\frac{i_{OQ1}(s)}{v_{bD1}(s)}$	$\frac{\omega_{PLL1}(s)}{v_{bD1}(s)}$	$\frac{\omega_{PLL2}(s)}{v_{bD1}(s)}$	$\frac{i_{OQ1}(s)}{v_{bQ1}(s)}$	$\frac{\omega_{PLL1}(s)}{v_{bQ1}(s)}$	$\frac{\omega_{PLL2}(s)}{v_{bD2}(s)}$
Without perturb	$\|error\|_{\delta(t)}$	352.629	674.491	171.121	83.197	83.624	48.148
	$\|error\|_{u(t)}$	5.667	5.891	1.134	2.077	1.362	1.732
	$\|error\|_{r(t)}$	32.283	33.675	2.875	0.315	2.604	6.670
With perturb	$\|error\|_{\delta(t)}$	433.935	732.271	129.016	15.633	65.836	29.346
	$\|error\|_{u(t)}$	6.311	2.583	0.279	0.095	14.035	0.508
	$\|error\|_{r(t)}$	166.138	29.647	0.275	0.410	0.604	4.919

The comparative analysis of the effects of MOR by proposed method with BT, in frequency domain, in terms of gain and phase margin are given in Table 4.5. It is clearly seen that the GM and PM of the reduced order model by the proposed method are close to that of the original system. Therefore, it can be said that, the results of reduced order modelling in time domain are equally applicable in frequency domain as the frequency domain features of the overall system remain close to that of original system.

Figure 4.10. represents the comparative analysis of the frequency response achieved by the proposed reduction technique as compared to the balanced truncation method. These magnitude plots of the optimal reduced order transfer function from input v_{bQ1} to output ω_{PLL12} , i_{oQ12}, give better approximation to the full order model till frequencies of 100 rad/sec. The phase plots can be seen to give best approximants till 10 rad/sec. The frequency analysis of reduced order model of perturbed system is not shown here as it will be much similar to that for unperturbed system, which is been analysed thoroughly in this work.

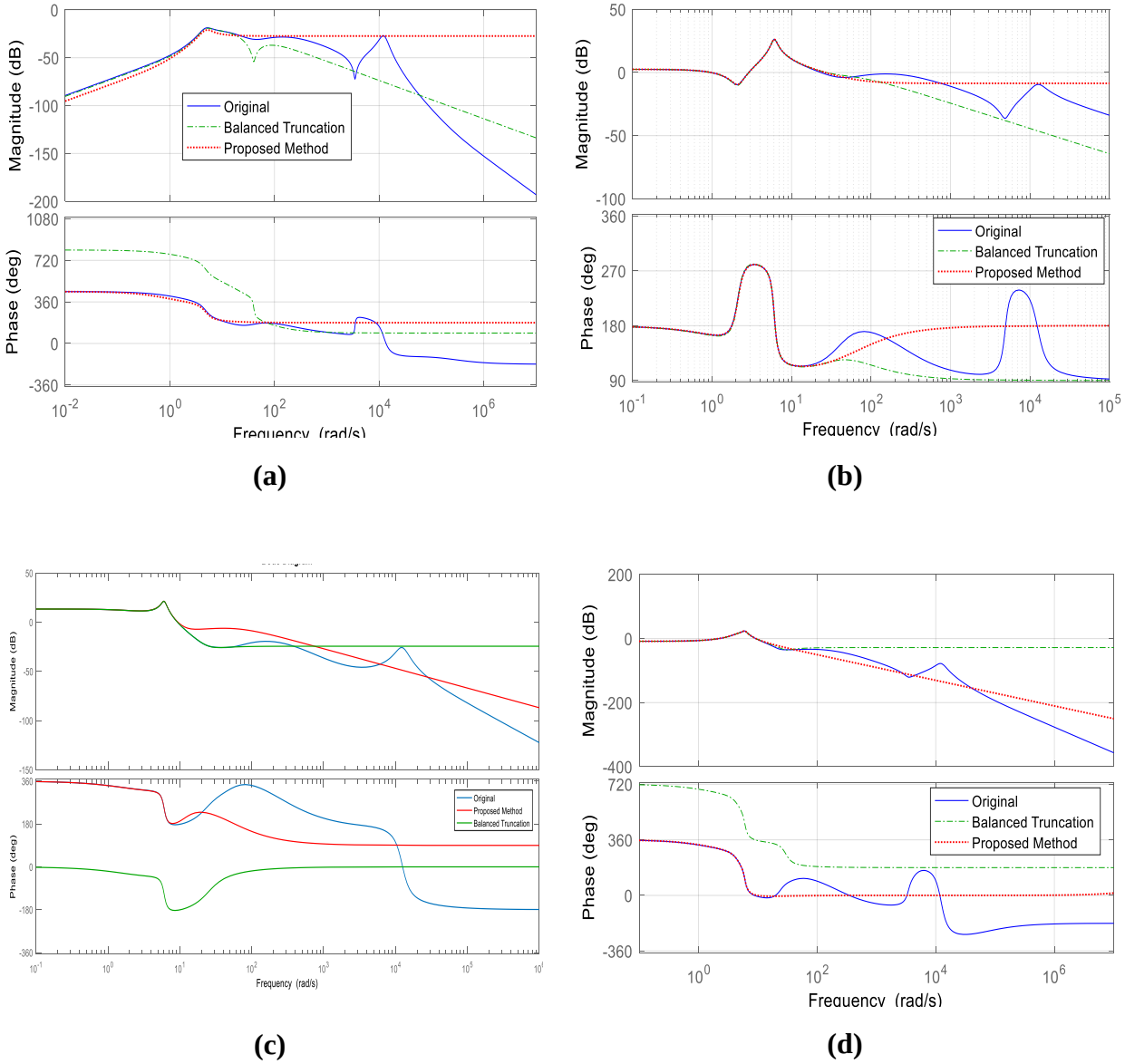

Figure 4.10. *Bodeplot of full order and reduced order transfer functions of autonomous microgrid.* (a) $\frac{i_{oQ1}(s)}{v_{bQ2}(s)}$, (b) $\frac{i_{oQ2}(s)}{v_{bQ1}(s)}$,(c) $\frac{\omega_{PLL1}(s)}{v_{bQ1}(s)}$,(d) $\frac{\omega_{PLL2}(s)}{v_{bQ1}(s)}$.

Table 4.5. Gain margin and phase margin of full order and reduced order autonomous microgrid.

Transfer Function	**Gain Margin**			**Phase Margin (degrees)**		
	Original	***BT***	***Proposed***	***Original***	***BT***	***Proposed***
$i_{OD1}(s)/v_{bD1}(s)$	0.82489	1.09702	0.82365	-23.62158	28.44517	-
$i_{OQ1}(s)/v_{bD1}(s)$	0.82774	0.84322	1.06409	25.94144	-25.48198	-
$i_{OD2}(s)/v_{bD1}(s)$	0.74987	0.70827	0.75015	-108.0896	-111.3116	-107.513
$i_{OQ2}(s)/v_{bD1}(s)$	1.58496	-	2.12825	-2.76498	6.24817	-1.77988
$\omega_{PLL1}(s)/v_{bD1}(s)$	0.74269	0.75544	0.74818	-1.31455	-124.3000	-1.26627
$\omega_{PLL2}(s)/v_{bD1}(s)$	0.19983	0.20343	0.20787	-23.06178	-20.54071	-18.7041
$i_{OD1}(s)/v_{bQ1}(s)$	0.55514	0.55089	0.55715	45.37122	45.62369	45.18011
$i_{OQ1}(s)/v_{bQ1}(s)$	0.57881	0.52184	0.65434	37.93962	48.88312	40.54128
$i_{OD2}(s)/v_{bQ1}(s)$	0.35861	0.35861	0.35858	-161.7277	-161.4156	-159.978
$i_{OQ2}(s)/v_{bQ1}(s)$	0.74939	0.74946	0.74931	-15.01546	-14.77873	-15.8253
$\omega_{PLL1}(s)/v_{bQ1}(s)$	0.09319	0.09360	0.09254	120.98238	121.89210	122.8886
$\omega_{PLL2}(s)/v_{bQ1}(s)$	0.75688	0.75551	0.75542	-73.20487	-72.74533	-73.6576
$i_{OQ1}(s)/v_{bD2}(s)$	4.36680	586.2070	9.68474	-	-	-
$\omega_{PLL1}(s)/v_{bD2}(s)$	1.47394	3.31899	2.51810	-	-	-
$\omega_{PLL2}(s)/v_{bD2}(s)$	16.78432	41.08055	1.25690	-	-	-
$i_{OQ1}(s)/v_{bQ2}(s)$	14.71627	13.23669	12.46060	-	-	-
$\omega_{PLL1}(s)/v_{bQ2}(s)$	0.31552	0.31545	0.31519	-1.46538	-145.4115	-13.1751
$\omega_{PLL2}(s)/v_{bQ2}(s)$	3.00617	3.32984	0.16855	-59.11295	-60.62443	-94.0979

3.3.1.2 Reduced order modelling of AC microgrid in grid-tied mode

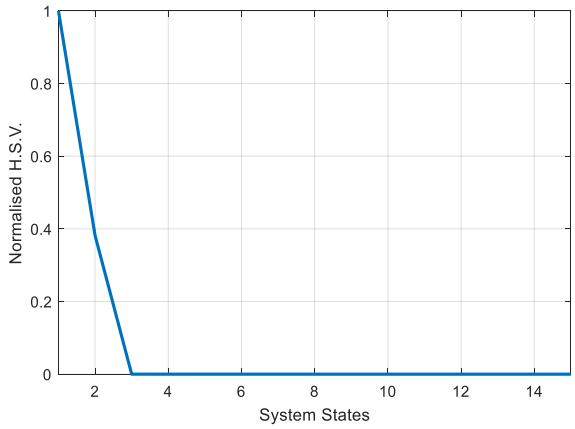

Figure 4.11. *HSV plot showing the energies of various states.*

The MIMO grid-tied microgrid system with nine outputs and two inputs is represented by the eighteen transfer functions as in (4.23). The normalised HSV plot of the system in Figure 4.11., shows, that two of the fifteen states have significantly large energy. Hence, the higher order system can be approximated by its 2nd order model without compromising system dynamic behaviour. Therefore, in this work, the 15th order transfer functions of the microgrid system are reduced to their 2nd order equivalent transfer functions by a number of traditional and advanced MOR methods. With two dominant poles, and considering pole retention technique with order of reduction, i.e., r as equal to 2, the common denominator with two eigenvalues of reduced order model is derived as, $Den_r(s) = s^2 + 0.000564833s + 0.00000071$.

The proposed reduction method is based on the intelligent and adaptive functionality of swarm-based ABC algorithm. Despite their equally intelligent approach, ABC is preferred over PSO algorithm in this analysis for reduced order modelling due to the following reasons which have been listed here and are proved by the simulation results.

Table 4.6. Parameters of the ABC Algorithm for AC microgrid in grid-tied mode

Parameter	***Value***
Colony size, n_c	40
No. of employed or onlooker bees, *N*	20
No. of runs, *Maxiter*	70
Limit	40
No. of dimensions in the particle, *d*	2

- Distributed control functionality in ABC in the form of three types of bees.
- A lesser number of parameters involved in this algorithm as compared to PSO where more number of variables affect the performance of optimization procedures.
- ABC Programming achieves the best fitness in 60-70 iterations, which is greatly reduced to 100-150 number of iterations in PSO for the same system.
- Faster optimization convergence and better fitness function values achieved by ABC makes it a better candidate for error minimization in MOR as compared to PSO.

The parameters used in the ABC algorithm are given in Table 4.6. The value of limit used in this paper is $0.5 \times d \times n_c$ ($n_c=2N$). The dimensions to be determined, i.e., *d*, is 2 as the numerator polynomial of the transfer functions to be computed by ABC have two unknown variables. The ISE and ITAE for order reduction of all the eighteen transfer functions by ABC based reduction method in comparison to that for direct truncation (DT), balanced truncation and PSO are given in Table 4.7. As seen from the table, results for ISE obtained for direct truncation for certain transfer functions like $\Delta P(s)/\Delta P^r(s)$, $\Delta Q(s)/\Delta P^r(s)$, $\Delta i_{ld}(s)/\Delta P^r(s)$, $\Delta Q(s)/\Delta Q^r(s)$ are not as bad as expected owing to the straightaway truncation of transfer function's numerator and denominator polynomials but their ITAE is very high as compared to other techniques. The magnitude

of approximation errors obtained by PSO and ABC algorithms are almost similar with negligible differences. However, ITAE obtained by the later method is observed to be better than former for most of the transfer functions. This table clearly indicates the superiority of the proposed methodology over other approaches due to the lower error parameters. Few of the time responses of the reduced order transfer functions of the grid-tied microgrid as in Figure 4.12. are seen to approximate the original full order system in a very accurate sense. The ramp responses for original and reduced order transfer functions $\Delta P(s)/\Delta P^r(s)$ and $\Delta Q(s)/\Delta Q^r(s)$ show that the approximations achieved by the combination method of the dominant pole with PSO and ABC, replicate the system effectively, and can thus be used in place of the original system for all analytical purposes.

Table 4.7.A ISE for all the transfer functions of grid-tied AC microgrid.

Transfer functions	***DT***	***BT***	***PSO***	***ABC***
$\Delta \boldsymbol{P}(\boldsymbol{s})/\Delta \boldsymbol{P^r}(\boldsymbol{s})$	0.0083	0.0040	0.0001	0.0000
$\Delta \boldsymbol{Q}(\boldsymbol{s})/\Delta \boldsymbol{P^r}(\boldsymbol{s})$	0.0002	0.0039	0.0002	0.0001
$\Delta \boldsymbol{i_{od}}(\boldsymbol{s})/\Delta \boldsymbol{P^r}(\boldsymbol{s})$	0.1226	0.0969	0.0033	0.0003
$\Delta \boldsymbol{i_{oq}}(\boldsymbol{s})/\Delta \boldsymbol{P^r}(\boldsymbol{s})$	284.0628	4.3365	0.7668	0.8483
$\Delta \boldsymbol{i_{ld}}(\boldsymbol{s})/\Delta \boldsymbol{P^r}(\boldsymbol{s})$	0.0854	0.0621	0.00001	0.0000
$\Delta \boldsymbol{i_{lq}}(\boldsymbol{s})/\Delta \boldsymbol{P^r}(\boldsymbol{s})$	284.5337	4.4619	0.7616	0.8820
$\Delta \boldsymbol{v_{od}}(\boldsymbol{s})/\Delta \boldsymbol{P^r}(\boldsymbol{s})$	6.7828	8.8611	7.9408	7.8129
$\Delta \boldsymbol{v_{oq}}(\boldsymbol{s})/\Delta \boldsymbol{P^r}(\boldsymbol{s})$	31.8653	17.8711	8.5576	8.9424
$\Delta \boldsymbol{\omega_{PLL}}(\boldsymbol{s})/\Delta \boldsymbol{P^r}(\boldsymbol{s})$	31.8653	17.2514	4.8295	5.1321
$\Delta \boldsymbol{P}(\boldsymbol{s})/\Delta \boldsymbol{Q^r}(\boldsymbol{s})$	38.8633	0.0009	0.00003	0.0000
$\Delta \boldsymbol{Q}(\boldsymbol{s})/\Delta \boldsymbol{Q^r}(\boldsymbol{s})$	0.0012	0.0012	0.0088	0.0004
$\Delta \boldsymbol{i_{od}}(\boldsymbol{s})/\Delta \boldsymbol{Q^r}(\boldsymbol{s})$	0.8595	5.2689	0.9473	0.9625
$\Delta \boldsymbol{i_{oq}}(\boldsymbol{s})/\Delta \boldsymbol{Q^r}(\boldsymbol{s})$	185.9666	1.2528	0.1283	0.0025
$\Delta \boldsymbol{i_{ld}}(\boldsymbol{s})/\Delta \boldsymbol{Q^r}(\boldsymbol{s})$	96.9943	0.4809	0.9032	0.9180
$\Delta \boldsymbol{i_{lq}}(\boldsymbol{s})/\Delta \boldsymbol{Q^r}(\boldsymbol{s})$	100.5219	0.0216	0.0062	0.0062
$\Delta \boldsymbol{v_{od}}(\boldsymbol{s})/\Delta \boldsymbol{Q^r}(\boldsymbol{s})$	393.7342	5.9710	6.3108	6.9939
$\Delta \boldsymbol{v_{oq}}(\boldsymbol{s})/\Delta \boldsymbol{Q^r}(\boldsymbol{s})$	36.8423	5.4816	17.1802	17.8962
$\Delta \boldsymbol{\omega_{PLL}}(\boldsymbol{s})/\Delta \boldsymbol{Q^r}(\boldsymbol{s})$	26.2396	5.2557	4.7121	16.2434

Table 4.7.B ITAE for all the transfer functions of grid-tied AC microgrid.

Transfer functions	*DT*	*BT*	*PSO*	*Proposed*
$\Delta \boldsymbol{P}(\boldsymbol{s})/\Delta \boldsymbol{P^r}(\boldsymbol{s})$	2253.2474	54.9980	5.22773	6.21890
$\Delta \boldsymbol{Q}(\boldsymbol{s})/\Delta \boldsymbol{P^r}(\boldsymbol{s})$	25867.1190	7.7414	11.01664	14.413112
$\Delta \boldsymbol{i_{od}}(\boldsymbol{s})/\Delta \boldsymbol{P^r}(\boldsymbol{s})$	498795.8691	3158.4796	1318.85658	18.56204
$\Delta \boldsymbol{i_{oq}}(\boldsymbol{s})/\Delta \boldsymbol{P^r}(\boldsymbol{s})$	367004.3119	3133.6406	2889.89704	1043.70617
$\Delta \boldsymbol{i_{ld}}(\boldsymbol{s})/\Delta \boldsymbol{P^r}(\boldsymbol{s})$	27565.6906	293.8888	30.27392	0.7654655
$\Delta \boldsymbol{i_{lq}}(\boldsymbol{s})/\Delta \boldsymbol{P^r}(\boldsymbol{s})$	367056.4205	2080.7764	2997.46198	1064.21921
$\Delta \boldsymbol{v_{od}}(\boldsymbol{s})/\Delta \boldsymbol{P^r}(\boldsymbol{s})$	400000.6511	821.4675	2107.95148	3169.08152
$\Delta \boldsymbol{v_{oq}}(\boldsymbol{s})/\Delta \boldsymbol{P^r}(\boldsymbol{s})$	116000.4672	4069.1691	2844.47710	3391.43323
$\Delta \boldsymbol{\omega_{PLL}}(\boldsymbol{s})/\Delta \boldsymbol{P^r}(\boldsymbol{s})$	529307.9874	1618.7208	4649.62045	2569.15894
$\Delta \boldsymbol{P}(\boldsymbol{s})/\Delta \boldsymbol{Q^r}(\boldsymbol{s})$	23233.9819	43.2233	30.71381	5.568207
$\Delta \boldsymbol{Q}(\boldsymbol{s})/\Delta \boldsymbol{Q^r}(\boldsymbol{s})$	227057.7749	130.4123	108.14163	22.20098
$\Delta \boldsymbol{i_{od}}(\boldsymbol{s})/\Delta \boldsymbol{Q^r}(\boldsymbol{s})$	309373.3383	4243.6088	1598.03400	1111.96216
$\Delta \boldsymbol{i_{oq}}(\boldsymbol{s})/\Delta \boldsymbol{Q^r}(\boldsymbol{s})$	238810.8271	1906.2481	1431.5790	56.42936
$\Delta \boldsymbol{i_{ld}}(\boldsymbol{s})/\Delta \boldsymbol{Q^r}(\boldsymbol{s})$	2225405.2058	2945.2861	1411.6475	1086.0060
$\Delta \boldsymbol{i_{lq}}(\boldsymbol{s})/\Delta \boldsymbol{Q^r}(\boldsymbol{s})$	1570128.9601	19035.0350	382.2398	88.79640
$\Delta \boldsymbol{v_{od}}(\boldsymbol{s})/\Delta \boldsymbol{Q^r}(\boldsymbol{s})$	4714508.1242	2484.1212	4116.4533	2998.5400
$\Delta \boldsymbol{v_{oq}}(\boldsymbol{s})/\Delta \boldsymbol{Q^r}(\boldsymbol{s})$	400267.4764	2898.8723	4528.8980	11503.29755
$\Delta \boldsymbol{\omega_{PLL}}(\boldsymbol{s})/\Delta \boldsymbol{Q^r}(\boldsymbol{s})$	2437041.0991	5277.5963	3705.1228	4569.74321

The step responses of higher order and reduced order transfer functions $\Delta i_{oq}(s)/\Delta Q^r(s)$ and $\Delta Q(s)/\Delta P^r(s)$ shown in Figure 4.12. (c) and (d) also prove the same. The sinusoidal responses of $\Delta i_{ld}(s)/\Delta Q^r(s)$ and $\Delta i_{ld}(s)/\Delta P^r(s)$ as shown in Figure 4.12. (e) and (f) gives almost similar responses for all reduction techniques. To be precise, the waveforms demonstrate that the reduced order transfer functions by ABC algorithm are closer to the original plot as compared to that of the PSO.

The reduced order model consists of two of the real eigenvalues of the full order model but duplicates the 15th order model with high accuracy. This simplified 2nd order model as compared to the original 15th order model is very easy to implement and work on.

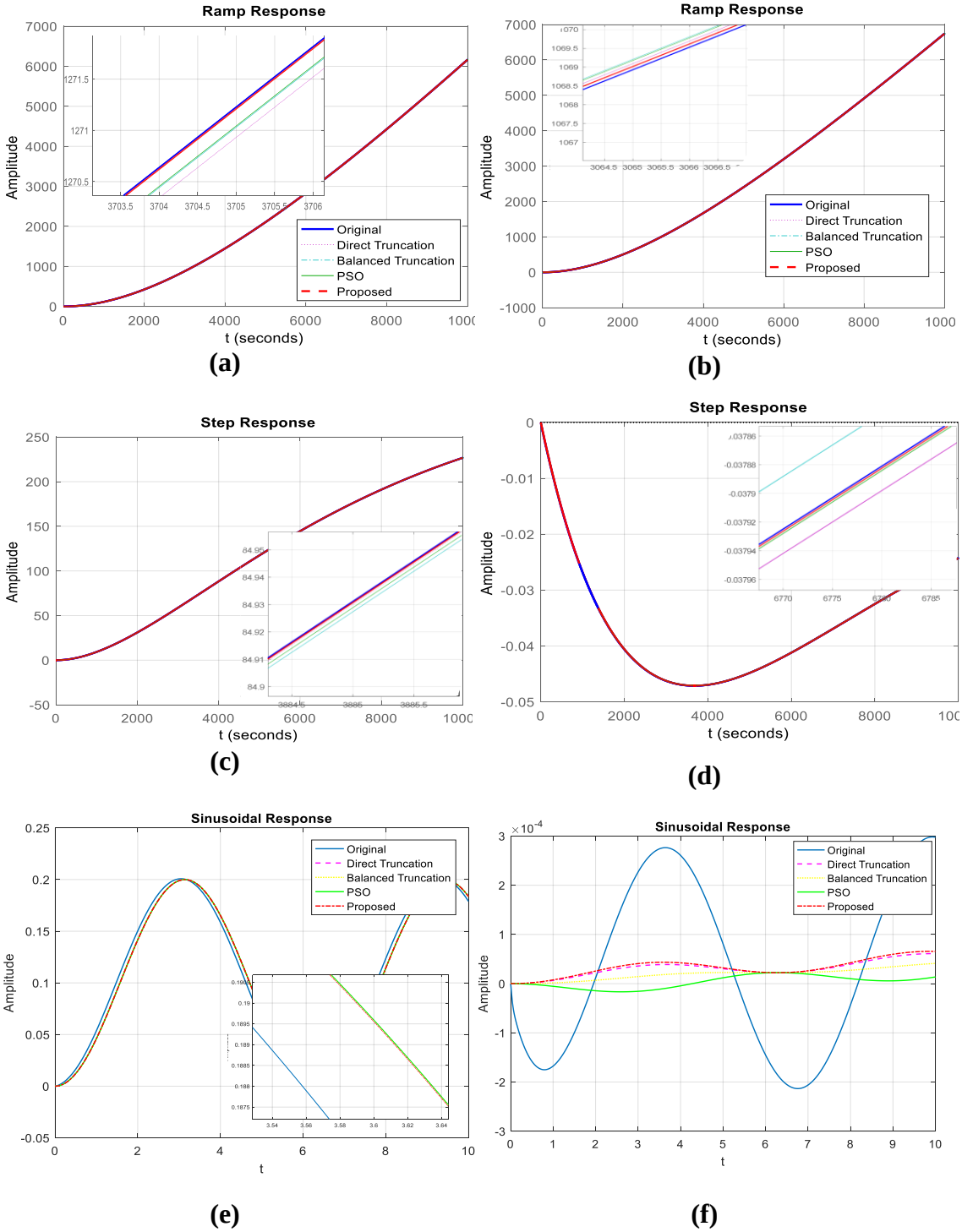

Figure 4.12. *Original and reduced order transfer functions of grid-tied microgrid. (a)* $\Delta P(s)/\Delta P^r(s)$, *(b)* $\Delta Q(s)/\Delta Q^r(s)$, *(c)* $\Delta i_{oq}(s)/\Delta Q^r(s)$, *(d)* $\Delta Q(s)/\Delta P^r(s)$, *(e)* $\Delta i_{ld}(s)/\Delta Q^r(s)$, *(f)* $\Delta i_{ld}(s)/\Delta P^r(s)$.

With ‘n’ number of DERs connected to the main grid at a point of time, the application of reduced order model for analysis will yield only ‘2n’ states to the overall model, which is much less than the ‘15n’ states by using full model. Thus the total reduction in number of states is by 86.667%.

Figure 4.13. gives the bode plot of two of the eighteen transfer functions to demonstrate the comparative analysis of the proposed method over other methods in terms of frequency. The original and reduced order transfer functions are compared in frequency domain plots to ensure the efficacy of the proposed reduction technique. As seen from this figure, the PSO and ABC optimized reduced models demonstrate similar behaviours at higher frequencies, but the ABC optimized reduced order model gives a better approximation to the original system than the PSO reduced models at low frequency. Further, a frequency domain analysis of the reduced order model in comparison to the full order system is quantitatively analysed in terms of the gain and phase margins for the transfer function model, and are given in Table 4.8.

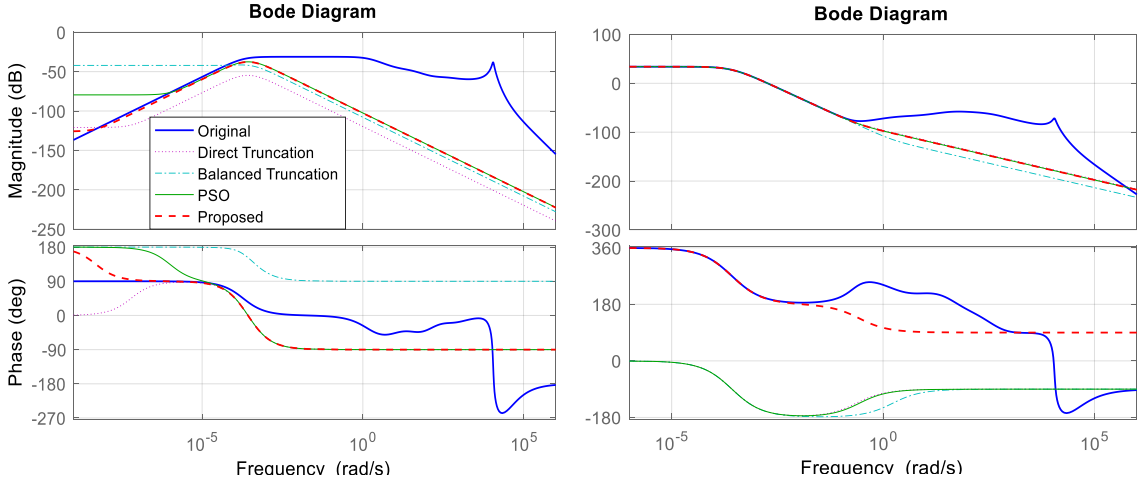

Figure 4.13. *Bode plot for full and reduced order transfer function of grid-tied microgrid (a)* $\Delta v_{od}(s)/\Delta P^r(s)$, *(b)* $\Delta i_{ld}(s)/\Delta P^r(s)$.

Table 4.8.A Gain margin of reduced order models in comparison to the original AC microgrid system in grid-tied mode.

Transfer functions	***Original***	***DT***	***BT***	***PSO***	***Proposed***
$\Delta \boldsymbol{P}(\boldsymbol{s})/\Delta \boldsymbol{P^r}(\boldsymbol{s})$	30.456	INF	INF	INF	INF
$\Delta \boldsymbol{Q}(\boldsymbol{s})/\Delta \boldsymbol{P^r}(\boldsymbol{s})$	15.9116	15.9129	15.9116	15.9116	15.9116
$\Delta \boldsymbol{i_{od}}(\boldsymbol{s})/\Delta \boldsymbol{P^r}(\boldsymbol{s})$	796.9801	INF	INF	INF	INF
$\Delta \boldsymbol{i_{oq}}(\boldsymbol{s})/\Delta \boldsymbol{P^r}(\boldsymbol{s})$	1403.0112	INF	INF	INF	INF
$\Delta \boldsymbol{i_{ld}}(\boldsymbol{s})/\Delta \boldsymbol{P^r}(\boldsymbol{s})$	783.1243	INF	INF	INF	INF
$\Delta \boldsymbol{i_{lq}}(\boldsymbol{s})/\Delta \boldsymbol{P^r}(\boldsymbol{s})$	INF	INF	INF	INF	INF
$\Delta \boldsymbol{v_{od}}(\boldsymbol{s})/\Delta \boldsymbol{P^r}(\boldsymbol{s})$	114.3281	INF	24492.9626	9459.7571	19685.9664
$\Delta \boldsymbol{v_{oq}}(\boldsymbol{s})/\Delta \boldsymbol{P^r}(\boldsymbol{s})$	INF	INF	INF	INF	INF
$\Delta \boldsymbol{\omega_{PLL}}(\boldsymbol{s})/\Delta \boldsymbol{P^r}(\boldsymbol{s})$	0.0034	0.0030	0.0034	0.0034	0.0034
$\Delta \boldsymbol{P}(\boldsymbol{s})/\Delta \boldsymbol{Q^r}(\boldsymbol{s})$	2.5243	2.5247	2.5244	2.5243	2.5243
$\Delta \boldsymbol{Q}(\boldsymbol{s})/\Delta \boldsymbol{Q^r}(\boldsymbol{s})$	70302.1219	INF	INF	INF	INF
$\Delta \boldsymbol{i_{od}}(\boldsymbol{s})/\Delta \boldsymbol{Q^r}(\boldsymbol{s})$	1386.8589	INF	INF	INF	INF
$\Delta \boldsymbol{i_{oq}}(\boldsymbol{s})/\Delta \boldsymbol{Q^r}(\boldsymbol{s})$	10.9961	INF	209.1839	336.8801	20.3370
$\Delta \boldsymbol{i_{ld}}(\boldsymbol{s})/\Delta \boldsymbol{Q^r}(\boldsymbol{s})$	INF	INF	INF	INF	INF
$\Delta \boldsymbol{i_{lq}}(\boldsymbol{s})/\Delta \boldsymbol{Q^r}(\boldsymbol{s})$	16037.9606	INF	217.6596	212.1416	11011.122
$\Delta \boldsymbol{v_{od}}(\boldsymbol{s})/\Delta \boldsymbol{Q^r}(\boldsymbol{s})$	INF	INF	INF	INF	INF
$\Delta \boldsymbol{v_{oq}}(\boldsymbol{s})/\Delta \boldsymbol{Q^r}(\boldsymbol{s})$	0.0049	0.0048	0.0048	0.0049	0.0049
$\Delta \boldsymbol{\omega_{PLL}}(\boldsymbol{s})/\Delta \boldsymbol{Q^r}(\boldsymbol{s})$	0.0019	0.0018	0.0019	0.0034	0.0019

The comparative analysis of frequency domain characteristics of the reduced order models in Table 4.8., clearly indicates that the proposed ABC based reduction technique

achieves good performance in the frequency domain in terms of gain and phase margins as compared to those of the original transfer functions.

Table 4.8.B Phase margin of reduced order models in comparison to the original AC microgrid system in grid-tied mode.

Transfer functions	***Original***	***DT***	***BT***	***PSO***	***Proposed***
$\Delta \boldsymbol{P}(\boldsymbol{s})/\Delta \boldsymbol{P^r}(\boldsymbol{s})$	INF	INF	-180	INF	INF
$\Delta \boldsymbol{Q}(\boldsymbol{s})/\Delta \boldsymbol{P^r}(\boldsymbol{s})$	INF	INF	INF	INF	INF
$\Delta \boldsymbol{i_{od}}(\boldsymbol{s})/\Delta \boldsymbol{P^r}(\boldsymbol{s})$	21.337	21.409	21.330	21.337	21.337
$\Delta \boldsymbol{i_{oq}}(\boldsymbol{s})/\Delta \boldsymbol{P^r}(\boldsymbol{s})$	90.667	90.145	90.667	90.145	90.646
$\Delta \boldsymbol{i_{ld}}(\boldsymbol{s})/\Delta \boldsymbol{P^r}(\boldsymbol{s})$	17.608	17.680	17.283	17.608	17.608
$\Delta \boldsymbol{i_{lq}}(\boldsymbol{s})/\Delta \boldsymbol{P^r}(\boldsymbol{s})$	90.676	90.145	90.006	90.145	90.645
$\Delta \boldsymbol{v_{od}}(\boldsymbol{s})/\Delta \boldsymbol{P^r}(\boldsymbol{s})$	INF	INF	INF	INF	INF
$\Delta \boldsymbol{v_{oq}}(\boldsymbol{s})/\Delta \boldsymbol{P^r}(\boldsymbol{s})$	92.653	90.956	90.956	90.956	92.653
$\Delta \boldsymbol{\omega_{PLL}}(\boldsymbol{s})/\Delta \boldsymbol{P^r}(\boldsymbol{s})$	-91.086	-89.80	-89.803	-89.803	-91.090
$\Delta \boldsymbol{P}(\boldsymbol{s})/\Delta \boldsymbol{Q^r}(\boldsymbol{s})$	INF	INF	INF	INF	INF
$\Delta \boldsymbol{Q}(\boldsymbol{s})/\Delta \boldsymbol{Q^r}(\boldsymbol{s})$	-180	INF	INF	INF	INF
$\Delta \boldsymbol{i_{od}}(\boldsymbol{s})/\Delta \boldsymbol{Q^r}(\boldsymbol{s})$	90.736	90.178	90.178	90.176	90.737
$\Delta \boldsymbol{i_{oq}}(\boldsymbol{s})/\Delta \boldsymbol{Q^r}(\boldsymbol{s})$	6.813	7.002	6.833	6.827	6.814
$\Delta \boldsymbol{i_{ld}}(\boldsymbol{s})/\Delta \boldsymbol{Q^r}(\boldsymbol{s})$	90.721	90.178	90.722	90.178	90.778
$\Delta \boldsymbol{i_{lq}}(\boldsymbol{s})/\Delta \boldsymbol{Q^r}(\boldsymbol{s})$	6.816	3.488	6.824	6.815	6.816
$\Delta \boldsymbol{v_{od}}(\boldsymbol{s})/\Delta \boldsymbol{Q^r}(\boldsymbol{s})$	INF	90.214	INF	90.214	INF
$\Delta \boldsymbol{v_{oq}}(\boldsymbol{s})/\Delta \boldsymbol{Q^r}(\boldsymbol{s})$	-92.150	-89.89	-88.722	-89.722	-90.722
$\Delta \boldsymbol{\omega_{PLL}}(\boldsymbol{s})/\Delta \boldsymbol{Q^r}(\boldsymbol{s})$	-92.171	-89.89	-89.892	-89.803	-91.902

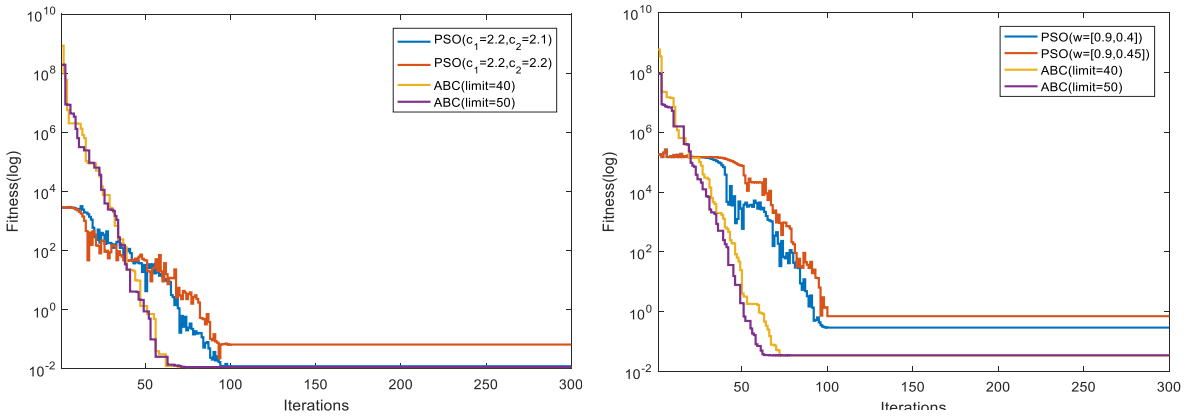

(a) **(b)**

Figure 4.14. *Convergence curve for PSO and ABC optimizations with parametric variations (a)* $\Delta P(s)/\Delta P^r(s)$, *(b)* $\Delta v_{od}(s)/\Delta P^r(s)$.

A statistical analysis of the fitness values obtained by optimization algorithm, i.e., PSO and ABC, in the form of mean, standard deviation and best fitness are tabulated in Table 4.9. The range of fitness values obtained in ABC based optimization in subsequent iterations is much more as compared to that for PSO algorithm. This can be seen from the high mean and standard deviation values for all transfer functions. The convergence curves for the PSO and ABC optimization algorithms for reduced order modelling of two of the transfer functions, $\Delta P(s)/\Delta P^r(s)$ and $\Delta v_{od}(s)/\Delta P^r(s)$, with changes in algorithm parameters, as in Figure 4.14., demonstrate the wide range of fitness values in ABC as compared to that in the PSO algorithm.

The faster convergence in terms of less number of iterations i.e. 60-70 iterations, to achieve the best fitness is clearly seen in the ABC based optimization as compared to the 100-110 iterations in the PSO algorithm, in both the transfer functions in spite of the changes in algorithm parameters. Table 4.9. also gives the best fitness and the average execution time for both the optimization algorithms.

Table 4.9. Statistical analysis of fitness values attained through PSO and ABC algorithm in each iteration and CPU time for optimization.

Transfer Function	*Mean fitness value ($\times 10^3$)*		*Standard deviation ($\times 10^3$)*		*Best fitness value*		*CPU time (sec)*	
	PSO	*ABC*	*PSO*	*ABC*	*PSO*	*ABC*	*PSO*	*ABC*
$\Delta \boldsymbol{P}(\boldsymbol{s})/\Delta \boldsymbol{P^r}(\boldsymbol{s})$	0.49	10.10	0.95	85.06	0.0124	0.0116	172.667	149.268
$\Delta \boldsymbol{Q}(\boldsymbol{s})/\Delta \boldsymbol{P^r}(\boldsymbol{s})$	16.59	5447.62	42.65	27463.93	0.0278	0.0271	164.907	140.772
$\Delta \boldsymbol{i_{od}}(\boldsymbol{s})/\Delta \boldsymbol{P^r}(\boldsymbol{s})$	58.29	208.11	73.52	680.96	0.2954	0.0349	163.961	137.969
$\Delta \boldsymbol{i_{oq}}(\boldsymbol{s})/\Delta \boldsymbol{P^r}(\boldsymbol{s})$	156.46	1610.96	317.01	6694.52	1.9627	1.9684	142.075	143.981
$\Delta \boldsymbol{i_{ld}}(\boldsymbol{s})/\Delta \boldsymbol{P^r}(\boldsymbol{s})$	14.97	12413.94	36.77	54971.79	0.0037	0.0012	155.555	139.386
$\Delta \boldsymbol{i_{lq}}(\boldsymbol{s})/\Delta \boldsymbol{P^r}(\boldsymbol{s})$	292.16	4398.33	488.89	29227.12	2.2633	2.0071	187.086	125.188
$\Delta \boldsymbol{v_{od}}(\boldsymbol{s})/\Delta \boldsymbol{P^r}(\boldsymbol{s})$	11.09	6532.74	23.82	56424.56	6.0565	5.9756	160.787	140.918
$\Delta \boldsymbol{v_{oq}}(\boldsymbol{s})/\Delta \boldsymbol{P^r}(\boldsymbol{s})$	22.87	5993.09	47.69	23588.24	6.4377	6.3929	161.438	149.491
$\Delta \boldsymbol{\omega_{PLL}}(\boldsymbol{s})/\Delta \boldsymbol{P^r}(\boldsymbol{s})$	256.27	6927.31	378.69	29087.38	4.3453	4.8434	153.127	130.126
$\Delta \boldsymbol{P}(\boldsymbol{s})/\Delta \boldsymbol{Q^r}(\boldsymbol{s})$	28.973	14702.72	65.74	88529.21	0.0106	0.0105	158.775	144.035
$\Delta \boldsymbol{Q}(\boldsymbol{s})/\Delta \boldsymbol{Q^r}(\boldsymbol{s})$	415.30	2209.32	959.11	11477.31	0.0562	0.0430	162.473	141.80
$\Delta \boldsymbol{i_{od}}(\boldsymbol{s})/\Delta \boldsymbol{Q^r}(\boldsymbol{s})$	314.72	14333.16	449.53	74421.17	2.1091	2.0968	160.452	144.916
$\Delta \boldsymbol{i_{oq}}(\boldsymbol{s})/\Delta \boldsymbol{Q^r}(\boldsymbol{s})$	275.56	3147.68	389.86	14001.87	1.4050	0.1072	159.621	142.132
$\Delta \boldsymbol{i_{ld}}(\boldsymbol{s})/\Delta \boldsymbol{Q^r}(\boldsymbol{s})$	287.58	3835.46	416.66	14724.36	2.1938	2.0476	159.066	140.871
$\Delta \boldsymbol{i_{lq}}(\boldsymbol{s})/\Delta \boldsymbol{Q^r}(\boldsymbol{s})$	164.77	1489.26	319.21	11234.72	0.2265	0.1679	159.464	140.022
$\Delta \boldsymbol{v_{od}}(\boldsymbol{s})/\Delta \boldsymbol{Q^r}(\boldsymbol{s})$	129.78	2190.93	256.20	9788.02	5.9189	5.6541	155.491	143.798
$\Delta \boldsymbol{v_{oq}}(\boldsymbol{s})/\Delta \boldsymbol{Q^r}(\boldsymbol{s})$	358.57	2329.95	375.93	13907.10	14.244	9.1734	156.724	140.923
$\Delta \boldsymbol{\omega_{PLL}}(\boldsymbol{s})/\Delta \boldsymbol{Q^r}(\boldsymbol{s})$	55.91	9056.29	138.20	85834.27	8.6798	8.6166	169.675	139.391

From these tabulations, it is worthy to mention that the reduced order modelling of grid-tied microgrid system by ABC algorithm is more advantageous than the PSO algorithm, in terms of both CPU time and fitness attained.

4.3.2 Optimal MOR in DC Microgrid

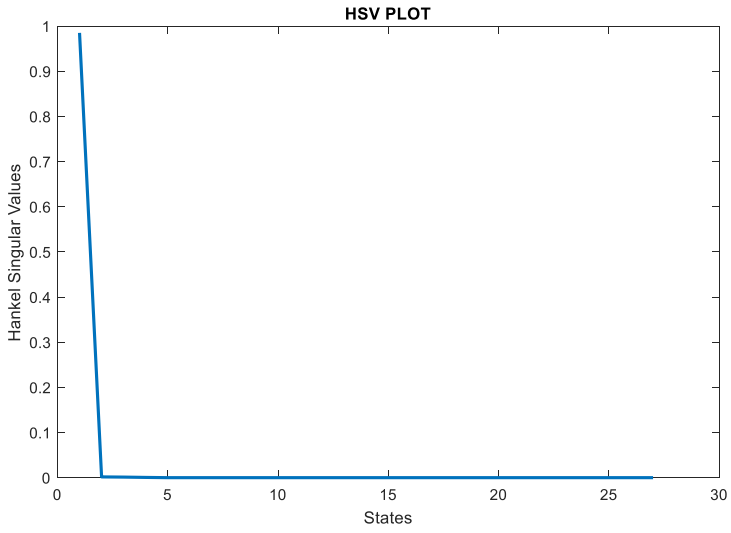

Figure 4.15. *Hankel singular values of 27 state fast subsystem*

In accordance with the flow of process for reduced order modelling of DC microgrid in Figure 4.4. by time scale separation using optimization algorithms, the order of the fast subsystem is reduced by PSO algorithm and then a the complete reduced order system is modelled as a combination of slow subsystem and reduced set of fast subsystem.

The Hankel Singular Value (HSV) plot of the fast subsystem is given in Figure 4.15. Since, HSV determines the highest energy states in the system, a single large value in the figure represents a single state with significant energy and thus, a single state reduced model, $x_{red,fast}$ will give a sufficient representation of 27 states of higher order state space representation, x_{fast}.

The MOR of the fast subsystem as in (28), is obtained through PSO algorithm code in MATLAB 2016a environment with fitness function in (33). The PSO algorithm parameters and obtained optimized state space values are given in Table 4.10. The hybrid norm for optimisation is determined to be with relative weights of $H_2 : H_\infty$ in the ratio of 3.2 : 1.

The response of the PSO h-norm based reduced model is compared with the balanced truncation reduced and original model as shown in Figure 4.16. This response shown is to the input which is abruptly varied twice from t=0 to 1200 seconds, such that unit step input is given for t=0 to 305 seconds; a 10% drop in input occurs at t=306 second and a 20% increase is given at t=701 second. The balanced truncated model can be seen to track transient response of full order model but a steady state error occurs which remains throughout the response. On the contrary the PSO reduced order model can be seen to track the load variations more accurately due to robust optimization function formulation.

The Table 4.11. given below enlists some of the characteristics of the full-order and reduced order models. The PSO reduced models depict mixed norm similar to full order model, and a decreased rise time and settling time. A negligible steady state error in PSO-reduced model as compared to the truncated one can be seen. PSO-reduced model clearly achieves a sufficient representation of the fast subsystem with a substantial reduction in system complexity in the form of reduced number of states by 26, and will be used in subsequent analysis of full system.

The overall simplified model of the DC microgrid is obtained as a combination of slow subsystem and reduced order representation of fast subsystem according to the principle of ‘peel-off and add back’ as mentioned in Section 4.2. This simplification in

modelling is achieved by retaining the significant system dynamics and discarding the fast ones.

Table 4.10. Optimization algorithm parameters and optimized values for DC microgrid.

Fixed Parameter	**Value**
Swarm size	40 particles
Iterations	100
$[c_1, c_2]$	[2.2,2.1]
w	[0.9,0.5]
Optimized variable	**Value**
$A_{red,fast}$	-0.01421
$B_{red,fast}$	[-0.08901 -0.16446 -0.00227 -0.00706 -0.00039 -1.22574 -1.64461 0.944142 -0.89014 1.64461]
$C_{red,fast}$	-0.94414
m	0.36642
n	0.11442

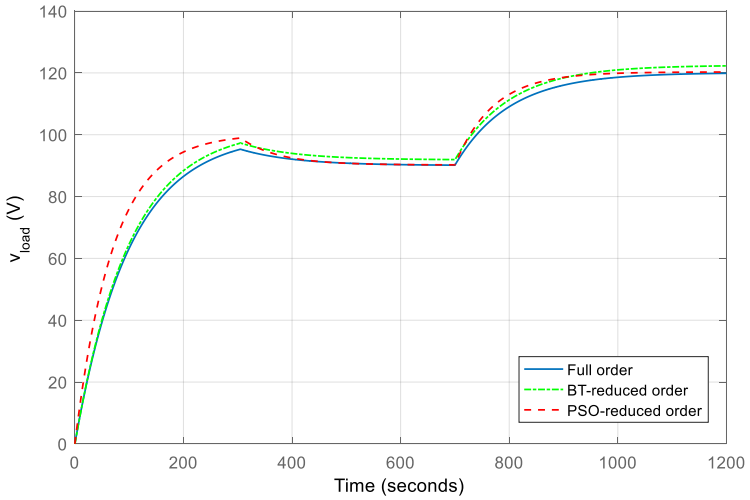

Figure 4.16. *Fast subsystem time response in DC microgrid.*

Table 4.11. Characteristics of fast subsystem of DC microgrid.

Fast Subsystem	***No. of States***	***Mixed h-norm***	***Rise time (sec)***	***Normalised peak amplitude(V)***	***Setting time (sec)***	***Steady state error(V)***
Full-order	27	26.6449	219.861	100.055	391.464	
BT reduced-order	1	27.0340	220.149	101.135	392.955	1.2
PSO reduced-order	1	26.4545	154.619	109.275	275.322	0.1

Table 4.12. enlists some important system characteristics of original and reduced order transfer functions, from output v_{load} to inputs, so as to compare their performances. Identical system properties ascertains the efficiency in reduction and accuracy in reduced order model to be used instead of its higher order counterpart in applications.

A case study of DC microgrid full-order and reduced-order system with changes in load and operating conditions is given below.

Table 4.12. System characteristics of original and reduced order DC microgrid

Transfer function from output v_{load} to input-	***Steady state error***	***GM(dB)***		***PM(deg)***		***Mixed h-norm***	
		Original	*Reduced*	*Original*	*Reduced*	*Original*	*Reduced*
i_{ccl}	0.40	61.9	inf	90.4	90.5	16.012	15.804
i_{ofc}	0.004	119	inf	inf	inf	0.631	0.598
i_{opv}	0.30	98.4	inf	106	104	0.071	0.053
e_{01}	0.30	61.6	inf	138	140	0.110	0.186
e_{02}	0.35	64.7	inf	inf	inf	0.110	0.059

CASE 1: Variation in load current sink, i_{cc}, in the following sequence: No load from 0 to 300 seconds; 50% decreased unit step input is abruptly applied at t=300; 4% reduced unit step input load is given for t=2800 to 4800 seconds; small random load changes are given for next 1200 seconds; 15% decreased unit step input load for last 4000 seconds.

The Figure 4.17. shows the load voltage variations when abrupt changes in load current sink according to the above sequence. The reduced model is seen to follow the instantaneous load changes with steady state value same as that achieved with the original model with 38 states. The model consisting of an approximate fuel cell closely follows the original system but varies in the steady state value.

CASE 2: Effect of variation of anode and cathode flow delay time λ_A, λ_C in fuel cell on the overall dynamics.

The flow of oxygen and hydrogen at cathode and anode respectively has no instant impact with respect to load variations. This inherent time delay is included as flow delay times, λ_A, λ_C in the fuel cell state space representation. The Figure 4.18. (a) shows a significant change in system temperature in range of -1200 K to 600K by variation of these delay times as 60 s, 120 s and 30 s. In addition to the inherent sluggish movement of these gases, a variation in flow delay times may occur due to obstructions in cell structure or gas supply variations etc. Slight deviations in these may remarkably affect the overall DC microgrid stability and control. The incorporation of full state space of fuel cell into the DC microgrid system will enhance monitoring these variations and hence can be controlled. Figure 4.18. (b) shows the changes in the 12^{th} state of the reduced model in order of 10^{-5} with changes in the electrode delay times as 60 s, 120 s and 30 s in fuel cell. It can be observed that it is insensitive to variations in electrode delay times as it dominantly retains the information of fast dynamics of DC microgrid system.

CASE 3: Effect of variation in disturbance input I by 10%

The variation in disturbance current from 0.1 ampere to 0.09 ampere does not impact the double-charge capacitor voltage, v_{cd} in reduced model much as shown in Figure 4.18. (c) whereas, the original model shows a large drift in capacitor voltage from 5 volts to 40-50 volts (changed polarity) with disturbance variations. Figure 4.18. (d) demonstrates the load voltage responses of the full-order, reduced-order and approximate fuel cell DC microgrid model with same variation in disturbance current. The steady state achieved by reduced model is same as that of full-order model whereas, the approximate model differs in steady state values to the original model.

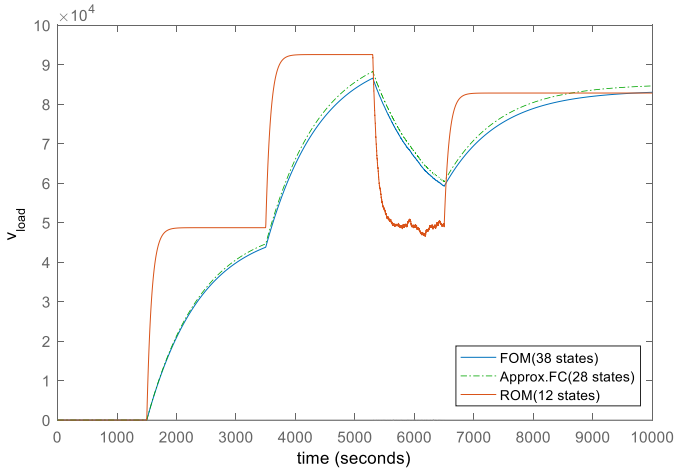

Figure 4.17. *Case 1: Load voltage variations on original, approximate and reduced order model.*

4.4 Real-time implementation with Typhoon HIL 402

The emulated grid-tied microgrid system has been accomplished in real-time, using Typhoon HIL 402, shown in Figure 4.19., where the circuit parameters are given in Table 4.13. Typhoon HIL 402 is a compact, real-time simulator with simulation step size in the range of microseconds and built-in 32 channel oscilloscope [90].

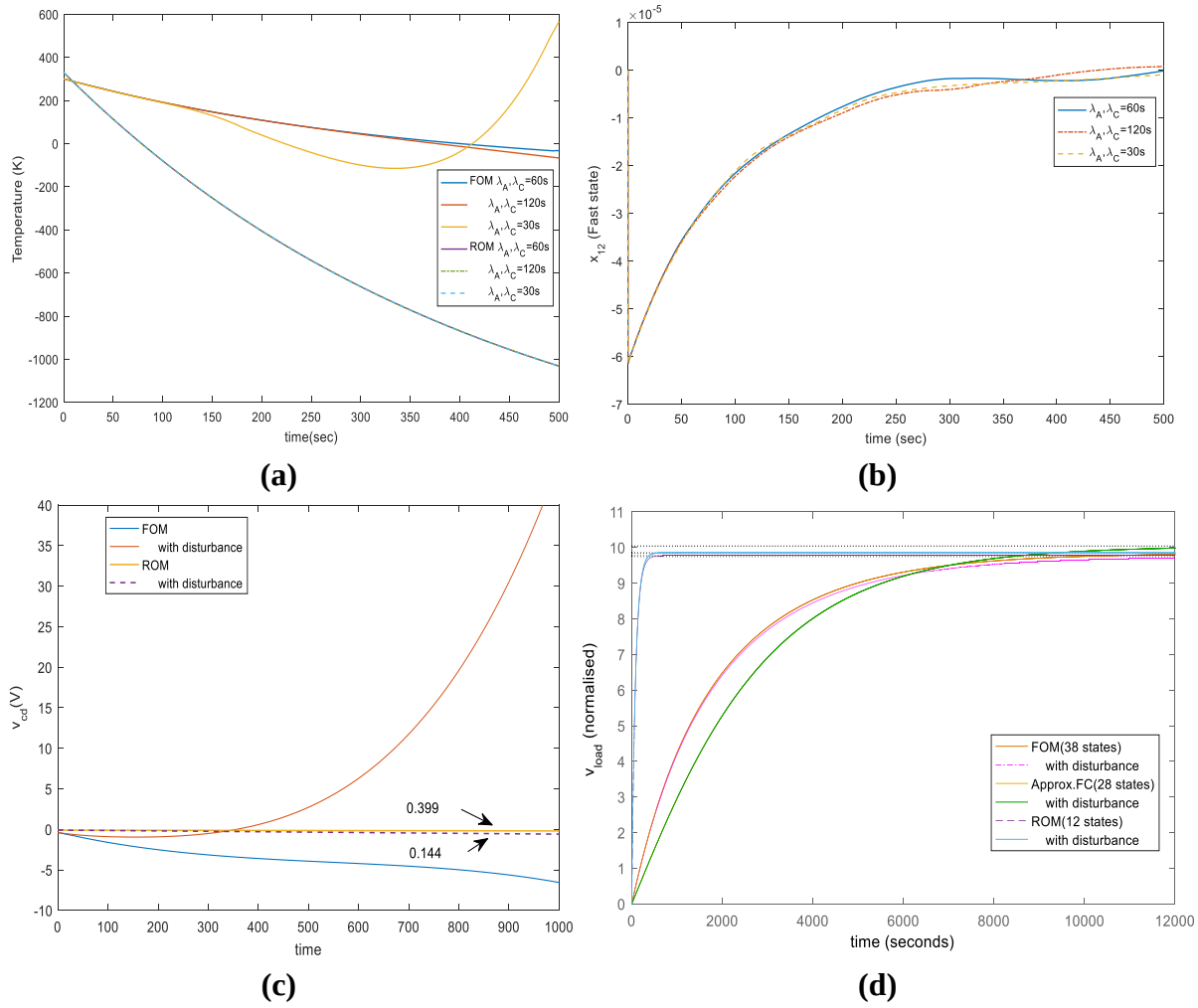

Figure 4.18. *Case 2: Effect of variation of anode and cathode delay time of fuel cell, (a) Effect on state, temperature, of full and reduced model, (b) Effect on state, x_{12}, of reduced model; Case 3: Effect of Variation in disturbance input, I, (c) Effect on double-charge capacitor voltage, v_{cd}, (d) Effect on output load voltage, v_{load} , full order and reduced order mode.*

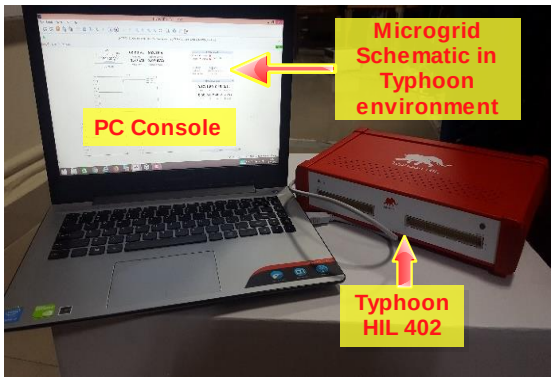

Figure 4.19. *Typhoon HIL 402 interfaced with console PC through USB cable.*

It provides a user-friendly software tool chain comprising of: (1) Control Center, for modelling and testing of systems; (2) Compiler, which rapidly converts model into processor readable description; (3) Processor, with low latency and high execution rate for fast implementation of converters and other associated elements in the microgrid.

Table 4.13. Specifications of components used in Typhoon schematic editor.

	Parameter	***Value***	***Parameter***	***Value***
Three phase inverter	Switching frequency	10 KHz	Nominal power	10 KVA
	Nominal voltage	480 V		
V_{dc}	Nominal DC voltage	1000 V		
PV Panel	PV plant area	5556 m^2	PV plant efficiency	20 %
Three phase two winding transformer	Rated power	5 MVA	Rated line to line voltage (Grid side)	13800 Vrms
	Rated frequency	60 Hz	Rated line to line voltage (Inverter side)	480 Vrms
LCL Filter	Inductance (inverter side)	4.2 mH	Shunt resistance	0.01568 Ω
	Resistance (inverter side)	1 μΩ	Shunt capacitor	1.51 mF
	Inductance (grid side)	0.6 mH		

The model for grid-tied microgrid system has been developed in the Typhoon HIL control center using the dedicated power system libraries available in the schematic editor. The host PC is connected to the typhoon 402 simulator through B-type connector USB 2.0 cable. The HIL SCADA interacts with the model in real time and provides a front panel for analysing microgrid operation without interrupting its operation.

The schematic model of the microgrid in grid-tied mode has been developed using a PV plant with a nominal voltage of 480 V, as a DG, connected to an inverter with switching frequency of 10 kHz as shown in Figure 4.20. The DG is connected to the grid through a filter, where the grid is modelled by a three-phase voltage source component. The offline optimized

reduced order transfer functions obtained through MATLAB program are modelled in Typhoon schematic editor as transfer function blocks available in its signal processing library.

The outputs obtained from the microgrid model and reduced transfer function blocks in the schematic editor are compared in real time with variations in inputs; P^r, Q^r and the results are shown in Figure 4.21. with a window length of 200 second duration.

Figure 4.21. (a) shows the output active power deviation, ΔP with changes in irradiation both in full order and PSO and ABC optimized reduced models. The irradiation changes from 1 W/m^2 to 1.5 W/m^2 at 40 seconds; and back to 1 W/m^2 at 80 seconds and finally reduced to 0.8 W/m^2 at 100 seconds. The reference power input of the state space model is considered as a function of solar irradiation for PV generation system which is an integral component of the microgrid system. The output active power of the original and reduced microgrid model are seen to track the changes in its reference value. Figure 4.21. (b) gives the output reactive power deviation, ΔQ with changes in reference reactive power, Q^r, such that it varies from 0.5 KVA to 0.7 kVA at 40 seconds; it further reduces to 0.4 kVA at 80 seconds; and gets back to 0.5 kVA at 100 seconds. The output reactive power of the original and reduced order models tracks the changes in reference values at every time instant.

Similarly, Figure 4.21. (c) shows the changes in d-axis output current, Δi_{od} with changes in irradiation, such that irradiation changes from 0.6 W/m^2 to 1.5 W/m^2 at 160 seconds when the time window is of 400 seconds. The output d-axis current from original and reduced order models track the changes in reference input with time. Figure 4.21. (d) gives the q-axis output current deviation, Δi_{oq} with changes in reference reactive power, Q^r in full order and reduced order models, such that it changes from 0.5 kVA to 0.4 kVA at 40 seconds; and to 0.7 kVA at 100 seconds. It is evident from these figures that the reduced order responses track the original system in real time with the ABC-reduced model demonstrating responses closer to the original system than the PSO-reduced models.

4.2 Summary

The 36^{th} order AC microgrid model in autonomous mode and 15^{th} order grid-tied model has been reduced to 9^{th} order and 2^{nd} order equivalent model with tolerable reduction errors. This reduced order model has been obtained through mixed methods of dominant pole retention and error minimization through PSO and ABC optimization techniques. Further, the system dynamics of the derived reduced order model is approximately same as that of its full-order model, which has been proved by time and frequency domain analysis and, hence the optimal reduced order model can be used in all small signal analysis, stability requirements and other controller requirements.

The reduced order model of PV-fuel cell based DC microgrid has been derived incorporating the principle of timescale separation. The state space model of the overall system consisting of 38 state variables obtained from individual component models, is grouped into the fast and slow subsystem, depending upon the response time of the states involved. The chemical-electrochemical phenomenon in fuel cell contribute to sluggish responses as compared to other electrical processes in the system. These sluggish states are grouped as slower subsystem and their high nonlinearities are retained intact in the reduced order model. Reduced order modelling of the fast subsystem extracts the key information to be included in the reduced order model along with the slow subsystem. This MOR of fast subsystem is obtained through mixed h-norm based PSO algorithm where the objective function is formulated as a weighted sum of H_2 and H_∞ error norms for obtaining efficient representation of original system with reduced tracking error and enhanced robustness.

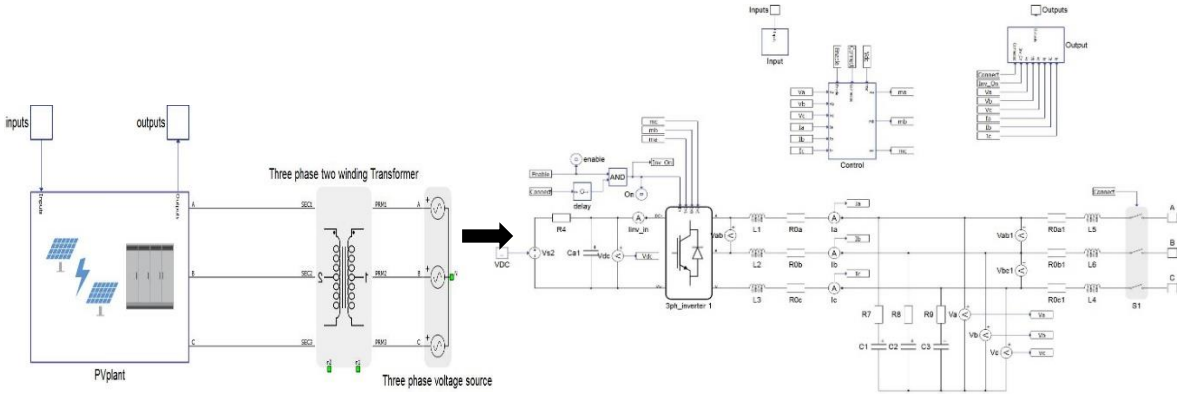

Figure 4.20. *Schematic of the grid-tied microgrid system in Typhoon HIL software.*

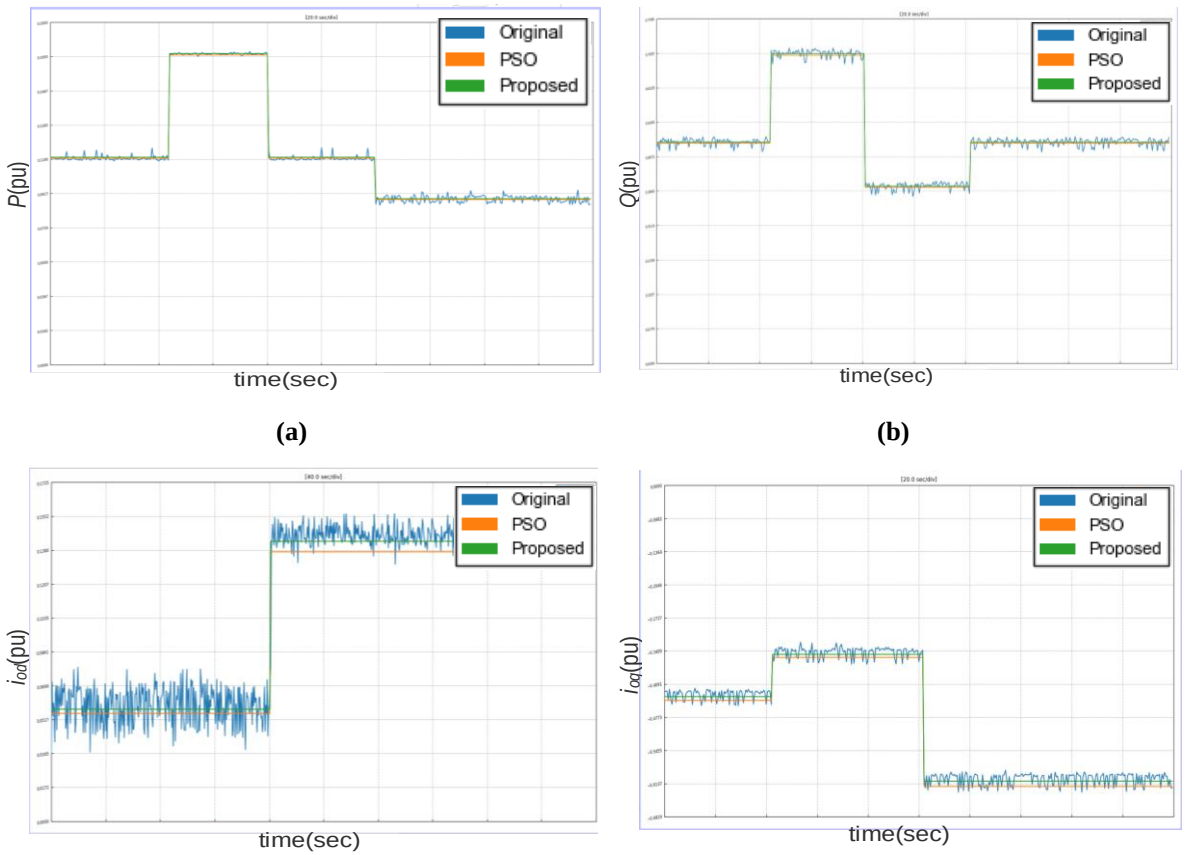

Figure 4.21. *Output responses of the original and reduced order system on Typhoon HIL platform (a) ΔP with changes in P^r; (b) ΔQ with changes in Q^r; (c) Δi_{od} with changes in P^r; (d) Δi_{oq} with changes in Q^r.*

(base values: 10 kW; 1 kVA; 10 A; 10A respectively)